Reconstructing Body Size and Center of Mass in Synapsids

Reconstructing Body Size and Center of Mass in Synapsids

Timothy Cavanaugh

A Thesis in the Field of Biology

for the Degree of Master of Liberal Arts in Extension Studies

Harvard University

November 2021

Abstract

Body size and center of mass of an organism have an influence on ecology, physiology, and locomotion. Vertebrates are typically preserved in the fossil record only as bones, so reconstructing their full body size requires estimation methods to account for soft tissue. Here, I employ two approaches in particular: volumetric reconstruction and limb scaling. Volume reconstructions were obtained through photogrammetry for an array of non-mammalian synapsids and therapsids in order to generate estimates of body mass and center of mass position. Secondary body mass estimates based on limb scaling were also computed using equations derived from Campione & Evans (2012). Comparison of volumetric and limb scaling approaches across 11 fossil tetrapods showed an overestimation of body mass range when using limb scaling equations, primarily due to the fact that early fossil synapsids have much more robust limb bones. Extant tetrapod limb bone diversity may not span the range of limb bone morphologies present in fossil species and may therefore be inadequate for inferring aspects of Synapsid biology. Further, the results here indicate all specimens likely employed quadrupedal locomotion, and normalized center of mass values are consistent with values observed in modern quadrupedal mammals. These findings contribute to our understanding of body size evolution in the forerunners of mammals and the methods best suited for estimating these characteristics.

Acknowledgments

I would first like to thank my thesis director Dr. Stephanie Pierce for allowing me to join the lab to work on this project, when I had little more than an appreciation for fossils and digital imaging. I am extremely appreciative for this opportunity to cap my experience performing research in (and out of) the lab. I would also like to acknowledge the Harvard Museum of Natural History, and the Museum of Comparative Zoology Vertebrate Paleontology Collections staff for their assistance with access to the specimens for photogrammetry and measurements. And finally, special thanks to Mark Wright, for patient and consistent advice and mentoring throughout this entire process.

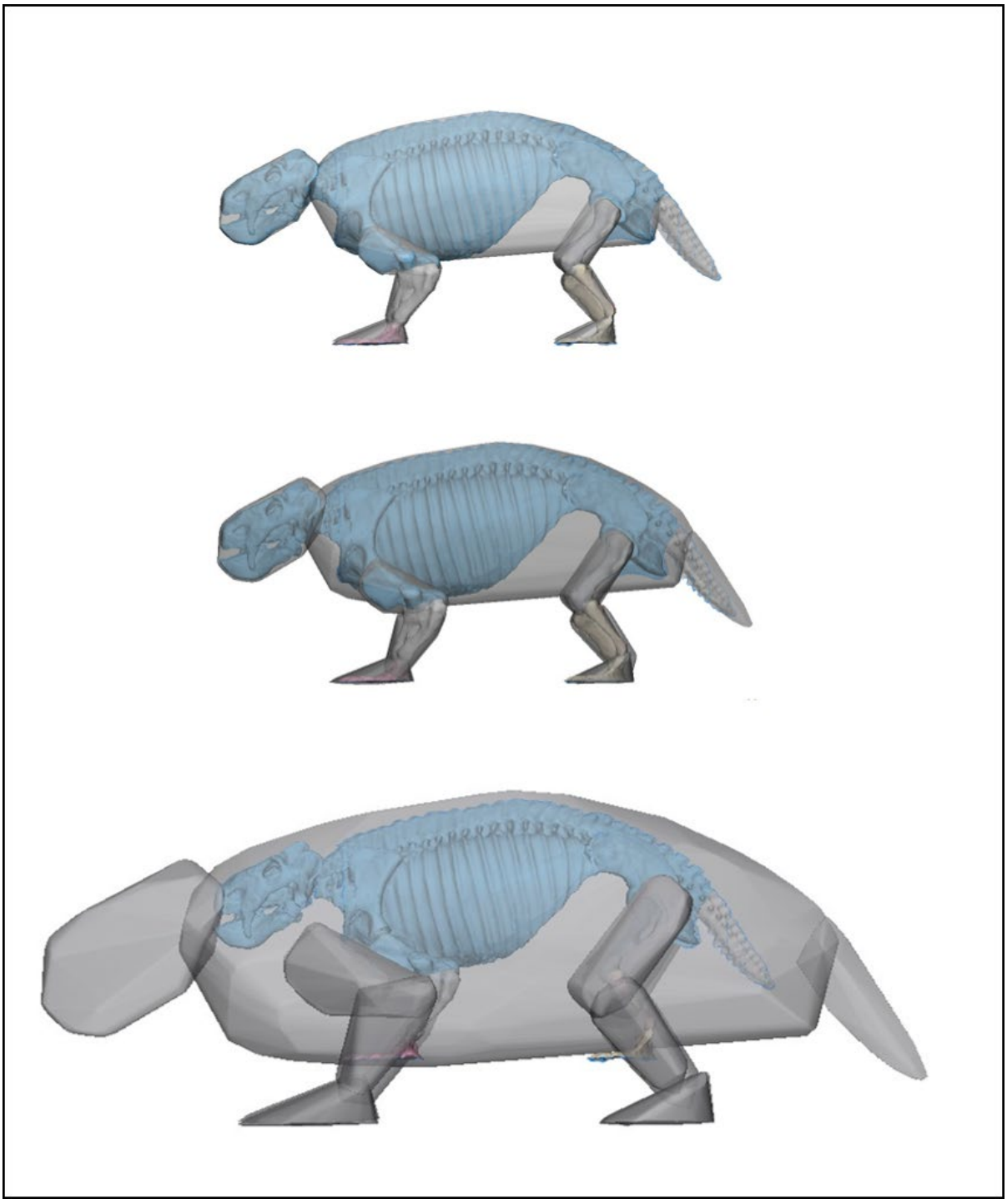

Table of Contents

List of Tables

List of Figures

I. Introduction

Evolution of Synapsids

Synapsids are a group of vertebrates that include modern mammals, as well as the extinct taxa that are more closely related to mammals than any other extant tetrapods. The history of synapsid evolution has been well-studied due to its importance to our understanding of modern-day mammals; this important lineage is supported by a reasonably clear and continuous fossil record that spans the development of early amphibious tetrapods and the subsequent divergence into the groups Sauropsida, comprising reptiles and their kin, and Synapsida, which includes extant therian mammals, marsupials, and monotremes, and their extinct forerunners. A rich taxonomic diversity of members of Synapsida that pre-date the first mammals are collectively referred to as "non-mammalian synapsids." Individual organisms in this lineage comprise many different forms and unique morphologies, and many traits that evolved in the non-mammalian synapsids have been conserved in the course of mammalian evolution (Kemp, 2005; Benton, 2009).

The non-mammalian synapsids, then, fill an important evolutionary space between the divergence of amniotes into Synapsida and Sauropsida and the emergence of crown mammals. The group of all synapsids that pre-dates therapsids, colloquially known as the "pelycosaurs," are represented by terrestrial quadrupeds with low postures and sprawling limb orientations, and, in some instances, elongated neural spines that supported a large dorsal sail as in the sphenacodontid *Dimetrodon*. Given the incompleteness of the earliest pelycosaur fossil record, the evolutionary relationship between members of the early synapsids has been mapped to various topologies. The earliest known synapsid species include the coeval *Archaeothryis*, an ophiacondontid, and *Echinerpeton*, whose taxonomic status is not fully resolved; both specimens are first observed in the fossil record in the late Carboniferous period, approximately 320 million years ago. Recent examination of newly

uncovered *Echinerpeton* remains suggest strongly that it also is classified most parsimoniously with the ophiacodontids (Mann & Paterson, 2019). Though these earliest known specimens are Ophiacodontidae, most recent phylogenies place Caseasauridae as the most basal synapsid family, with Varanopidae forming either a basal member or sister taxon to the more derived Eupelycosauria (Kemp, 2005).

What is universally accepted is that the non-mammalian synapsid lineage expanded throughout the Permian, with more derived species displaying both an increasing adaptation to terrestrial environment and more refined skull shape and dentition (Kemp, 2005). Members of these early, pelycosaur synapsids evolved to fill varied ecological niches and maintained diverse dietary habits; each pelycosaur family included individual species with large body size while individual specimens were variously carnivorous, insectivorous, piscivorous, herbivorous, or omnivorous (Reisz & Frobisch, 2014; Benton, 2009; Kemp, 2005).

The emergence of the more advanced monophyletic group Therapsida from a sphenacodontid ancestor is represented in the fossil record by a diversity of species with overall stronger jaw muscles, longer, more gracile limbs, and increasingly upright postures, with many species having semi-sprawling to semi-erect posture, or the ability to switch between sprawling and more upright limb positions (Kemp, 2005). The therapsid clade radiated widely throughout the later Permian and Mesozoic, and includes the crown group mammals that are first observed in the latest Triassic (Luo, 2007).

Limb posture and gait are critical body parameters for understanding an animal's capability for locomotion and dietary ecology, and major evolutionary shifts in these traits occurred between the earliest tetrapods and the first mammals (Regneault & Pierce, 2018). Many of the most basal tetrapods are understood to be semi-aquatic, with short sprawling limbs capable of only a very limited range of motion and permitting a "dragging" type gait along a muddy substrate in sub-aqueous to para-terrestrial environments (Ahlberg, *et al.*

20015; Pierce, *et al.* 2012). While non-mammalian synapsids were capable of terrestrial locomotion, their gait remained sprawling, with abducted limb posture and the belly held close to the ground (Benton, 2009). Furthermore, these early synapsids encountered restrictions to limb mobility and range of motion, owing to their bulky, "screw-shaped" pectoral girdles and short, robust stylopodia (Kemp, 2005)

Posture and gait evolved from a low-slung, reptilian appearance in the pelycosaur synapsids to a more upright, parasagittal limb build by the emergence of the earliest mammals. The upright posture may have evolved independently multiple times during the history of synapsids, with some later cynodont therapsids possibly capable of both sprawling and parasagittal postures (de Oliveira and Schultz, 2015). Gradual postural shifts have been observed beginning with primitive dinocephalian therapsids in the late Permian. Dinocephalians are believed to be one of the most basal therapsids; among these, *Moschops*, has hindlimbs in "derived, erect posture," but the posture of the long forelimbs is sprawling (Benton 2009). This semi-derived limb posture resulted in an animal that could possibly switch posture, though Kemp (2005) postulates that based on the large body size of most dinocephalian therapsids, "a more or less fully erect gait was obligatory." Later cynodont therapsids, notably *Thrinaxodon,* display a semi-sprawling stance, due to pelvic girdle innovations and more closely tucked hindlimbs (Damiani et al 2003; Benton, 2009). Since no extant mammals can provide information about these important early evolutionary transitions, studying the non-mammalian synapsids and other extinct taxa can fill in these gaps in our understanding.

Body Mass Estimation

The mass of an organism is critical to understanding the physiological traits and life habits of a given species, and vertebrate paleontologists have long sought to estimate body mass information from extinct organisms using different methods in two main categories: a volumetric approach, to estimate the volume of an organism and, by using an inferred body density, its mass; or an allometric approach, modeling body mass based on some other easily obtained physical measurement from the specimen. An early volumetric approach by Gregory (1905) involved hand-sculpting a $1/16^{th}$ scale model of a *Brontosaurus* in clay and performing displacement experiments in water to estimate the animal's volume and, by extension, its mass. Romer (1940) developed an early allometric ratio in "pelycosaurs"; by interpreting the vertebrae of an organism as a major weight-bearing structure, he determined that the cross-sectional area of a section of the vertebral column should be able to be cubically scaled to form a relationship with body mass. The advent of digital imaging and three-dimensional reconstruction methods as well as the availability of specimens and then development of new modeling techniques have led to advancements to these two main approaches for body mass estimation.

The first method, using an allometric relationship between body mass and limb diameter, suggests that the capability of an organism to support a given body mass is dependent on the robustness of its limb bones as defined by the minimum diameter of the humerus and femur. Campione and Evans (2012) developed robust predictive equations for a wide range of extant mammalian and reptilian specimens using minimum limb bone diameter and measured body mass. This approach is attractive for fossil specimens for several reasons. This method is comparatively simple to implement, requiring only a scale to measure body mass and a ruler for measuring limb diameter in a series of extant animals. Once a sufficient number of animals have been measured for limb diameter and body mass, a curve can be

calibrated to establish the relationship between these parameters; if the animals used for calibration are suitably similar to the fossil, it is then simply a matter of measuring the fossil limb diameters and predicting a body mass from the data set. This can be achieved rapidly for a large number of fossil bones, and little interpretation is required regarding factors such as fleshiness or muscle mass. Finally, since most fossil organisms are not completely preserved, this method permits a body mass estimation from only one or two bones, which greatly expands the number of specimens that can be analyzed with this technique.

By collecting data from a large number of specimens, the limb scaling method can demonstrate a fast and easy approach to estimating body mass in an unknown organism using a regression line to correlate the measured limb dimension to a measured body mass database. By necessity, the individual specimens that are used to calibrate this method must be living organisms so that an accurate body mass can be recorded; therefore, there is some risk when fitting extinct species to the regression line. Additionally, some species may simply be outliers to a line of best fit for a specific taxon based on individual or distinctive morphological characteristics. Basu (2016) highlights the risk of relying on only one or two bone dimensions to accurately predict the mass of the extinct ruminant mammal *Sivatherium giganteum;* to support its massive, oversized antlers, *Sivatherium* developed extremely robust forelimbs that do not correspond to an overall increase in body mass. By using the forelimb dimension as a variable, the whole-body mass will likely be overestimated. Similarly, Bates (2015) examined a specimen of *Dreadnoughtus,* a sauropod dinosaur of very large size, and found that applying a conventional limb scaling method for body mass estimation yields an overestimation of body mass between 36 and 63% when compared to volumetric density estimates. More recently, and relevant to the non-mammalian synapsid clade, Romano and Rubidge (2019) and Romano and Manucci (2019) examined two large bodied extinct Therapsids using a limb-scaling and volumetric approach, and found that in order to match

the large body mass predicted by the limb scaling based on stylopod circumference, the animals would have had to maintain a total body density of 1590-2300 kg/m3, values more congruent with some minerals than any known vertebrate.

In response to repeated observances of discrepancy between volumetric density reconstructions and the application of limb scaling estimates, particularly in regard to large animals with robust limbs, Campione (2017) proposed a second-order polynomial equation designed to yield lower size estimates for organisms that have larger body mass than the extant mammals and reptiles used to generate the lib scaling curve. Most recently, Campione and Evans (2020) compiled a comprehensive review of the two approaches, with specific regard to estimating the mass of non-avian dinosaurs. The authors conclude that where both models are applicable, 73% of volumetric body mass estimates fall within the 95% confidence interval predicted by limb scaling; of those that do not nearly "three quarters of outliers occur below the lower 95% prediction interval".

Finally, the limb-scaling approach yields only one parameter, an estimate of body mass, and cannot be used to determine any information regarding mass distribution in the organism, surface area, or other total body statistic.

A second common method of estimating body mass from fossil remains involves the three-dimensional scanning of a complete skeleton and digital processing to create a convex hull, a geometric minimum shape that encloses all of the points of the skeleton (Figure 1). Creating a convex hull is sometimes referred to as "shrink-wrapping," (Brassey, 2017), since the resulting object is wrapped tightly around the skeleton, and does not reflect the presence of muscle mass or soft tissue from the organism.

The process of creating a convex hull from a fossil specimen is most often accomplished in visualization software by creating a three-dimensional mesh object representing the convex hulls of each functional body segment of a scanned organism. If the

set of convex hulls created represents the minimum body volume of the organism, then a body mass can be estimated by applying the equation [mass = volume * density]. The density scalar can be altered to provide a range of possible body mass values based on the organism in question, its taxonomic classification, and assumptions about its habits. For example, a reconstructed model of an extinct reptile with presumed semi-aquatic habits could be modeled with a body density similar to an extant crocodile or other similar organism. Bates (2015) in a reconstruction of sauropod dinosaurs utilized an overall body density of 791-900 kg/m^3; Sellers (2012) utilizes a mean body density of 893 kg/m^3 based on a prior study of horse body segment density. Body mass estimation from digitized specimens is therefore often presented as a range of minimum and maximum values, to account for the amount of interpretation regarding fleshiness, differences in body segment density, presence of air sacs within the torso, or other factors.

Since the convex hull created from a fossil skeleton is considered the minimum body volume, simply using that volume, and multiplying by a density scalar will likely underestimate an accurate body mass from life. Brassey and Sellers (2014), in an overview of different approaches to fossil mass reconstruction, suggest that rather than directly estimating mass from a convex hull volume, a calibration curve should be generated for minimum convex hull volumes and body mass of modern specimens similar to the fossilized animals of unknown mass.

Work by Brassey et al. (2015), Bates et al. (2015), and Basu et al. (2016), among others, has shown consistent discrepancy between using a bivariate limb scaling methodology or a convex hull volumetric estimate of body mass in extinct organisms. Sellers et al. (2012) showed that in large mammals, simply using the convex hull method yielded body mass values approximately 21% lower than other approaches. The sources of error described

above, as well as the requirement for a fully preserved skeleton for digitization, are hurdles to widespread use of this technique.

Successful digitization and volumetric calculation of an extinct specimen relies on a high-quality three-dimensional data set, which is typically acquired through computed tomography (CT), laser scanning, or photogrammetry. Depending on the condition of the specimen, significant digital manipulation of the scanned object may be required, to correct for issues such as distortion, missing bones, or even a complete re-articulation of individually scanned bones.

Center of Mass Estimation

In addition to body mass, volumetric reconstructions also permit the calculation of an animal's whole body and individual body segment center of mass values. Allen et al. (2009) demonstrates the importance of the center of mass of a specimen for understanding posture and gait yet stresses that the accuracy of quantitative COM values have been poorly studied.

Center of mass estimation from digitized specimens has been used to infer the locomotor behavior of an organism. Mallison (2010) reconstructed the center of mass from a *Plateosaur* and determined that it likely walked bipedally. Nyakatura, et al. (2015) modeled the center of mass in conjunction with joint mobility analysis for the early diadectid, *Orobates pabsti*, to predict that the organism walked quadrupedally with the hindlimbs providing the majority of the locomotor force. Center of mass estimation has also been used to track shifts in ontogenetic locomotor patterns. Otero et al. (2019) studied several preserved species of *Mussaurus* at different stages of ontogenetic development and determined that the organism transitioned from quadrupedalism as a hatchling to bipedalism in adulthood, and related these locomotor changes to demonstrated posterior shift in center of mass.

Published methods for calculating center of mass vary; for example, the referenced *Plateosaur* study by Mallison uses a finite element analysis algorithm within a CAD software program to measure the center of volume of a three-dimensional digitized model of a mounted specimen. The method used by Nyakatura to estimate center of mass from the *Orobates* specimen is more detailed; the digitized specimen is divided into functional segments and then center of mass of each individual segment is measured using a custom MATLAB script (Nyakatura et al. 2015, supplemental information). Finally, the whole-body center of mass can be calculated from a summation of the individual segment CoM values multiplied by their distance from the system origin of the model.

The broad aim of this study is to compare the two methods of body size estimation to improve our understanding of body size evolution in synapsids.. Given prior observations that volumetric density and limb scaling approaches produce divergent ranges of mass estimates in fossil taxa, special attention is given to assessing the suitability of each approach for the members of the synapsid lineage included here. Basal synapsids are interpreted to be obligate sprawlers; quantitative assessment of the center of mass results will be investigated in this context, and in comparison to modern quadrupedal mammals.

II. Materials and Methods

Selected Specimens for Body Size Analysis

A total of nine fossil specimens are included in the digital modelling and reconstruction dataset for this study; including six specimens digitized for the first time here through photogrammetry (Table 1). All specimens are contained in museum collections and have been described previously in the literature. In order to increase the taxonomic breadth of the study, additional models were incorporated into the body mass and center of mass modelling dataset by utilizing a combination of previously digitized fossil specimens and an open-access digital model from another research group (Table 1). Beyond the incorporation of these additional digital models, the dataset was also expanded to include estimates of body mass from relevant taxonomic groups previously published in the literature, but where no digital models were available.

Initially, six specimens were selected from the collections of the Harvard Museum of Comparative Zoology (MCZ) for digitization through photogrammetry and body mass reconstruction. Each of these specimens is currently on display in the Harvard Museum of Natural History (HMNH) in a posed, lateral view, such that only half of each skeleton can be photographed. The species selected span a range of tetrapods that pre-date the evolution of Mammalia: the individuals include a primitive amphibian (temnospondyl); a member of the Diadectidae (considered stem amniotes; Laurin and Reisz, 1995); three non-mammalian "pelycosaur" synapsids; and a dicynodont therapsid *Dinodontosaurus turpior* (Table 1).

This model set was expanded by incorporating a previously acquired photogrammetric model of the early cynodont therapsid *Procynosuchus delaharpeae*; a skeletal reconstruction of the therocephalian therapsid *Scaloposaurus punctatus* that had

previously undergone CT-scanning and fully assembled for the first time in this study; and one CT-scan derived model of the basal diadectid *Orobates pabsti* obtained through open access from the authors of Nyakatura *et al* (2015). Figure 2 displays the phylogenetic relationship of the sample set. Finally, published body volume reconstruction and limb dimension measurements from the literature for the dinocephalian therapsid *Tapinocaninus pamelae* and the dicynodont therapsid *Lisowicia bojani* were used to calculate body mass estimates using the same workflow and equations (Romano & Rubidge, 2019; Romano & Manucci, 2019).

Photogrammetry and Reconstructions

Each photogrammetry dataset consists of between 50-200 digital photographs of a single specimen from multiple heights and orientations in order to capture all angles of the skeleton, to promote accurate reconstruction of the photogram, including more accurate image stitching, enhanced surface details and minimizing the effect of uneven illumination. The photographs were acquired in JPEG format with a Nikon D3300 digital camera using automated settings for aperture size, exposure time and ISO to account for changes in illumination caused by varying orientation of the specimen display cases in the museum hall. For each specimen, three data sets were acquired: 1) Full skeleton as posed; 2) post-cranial skeleton only with the skull removed; and 3) Isolated skull only. The datasets for the skull were captured in three poses on a turntable: dorsal, right lateral, and left lateral, and the three poses integrated into a single skull reconstruction. For Eryops, only dorsal and ventral datasets were acquired as the skull is dorsoventrally flattened. For Dinodontosaurus, it was not possible to remove the skull so only the full skeleton data set was acquired along with additional high-resolution images of the skull in its mounted position.

Following the acquisition of the photographic datasets, the images were rendered into a 3-dimensional photogram using Agisoft Photoscan (Agisoft LLC, Russia). Photographs were aligned in this program based on overlapping waypoints in each photo, and then used to generate a dense point cloud followed by a polygonal mesh model. This mesh model was then exported as a 3-dimensional object file (OBJ) for further processing.

Further reconstruction of the three-dimensional mesh was then performed using a combination of one or more software packages, including Meshlab (Cignoni, 2008) and 3-Matic (Materialise NV, Leuven, Belgium). The process of reconstruction involved several steps. For each specimen, a number of background elements were removed from the object file, including textual information from the display case, shadows, and other extraneous pixels. Since each specimen was mounted in profile view in its display case, the 3-dimensional model produced from the photogram was mirrored in order to reproduce the missing half of the skeleton; therefore, each half-skeleton can be duplicated and then mirrored to produce one entire skeletal model. Because each specimen was mounted in a lifelike, "posed" position, there were specimen-specific issues regarding tail curvature and skull orientation. In most cases, following the duplication and mirroring, some elements of the skull and tail required rotation and realignment to the principal body axis. Finally, the completed models were aligned to the world coordinate system with the tip of the snout touching the center of the cartesian coordinate space (0,0,0), and the X-axis corresponds to the mediolateral axis (X+=dextral, X-=sinistral), the Y-axis to the craniocaudal axis (Y+=cranial, Y-=caudal), and Z-axis to the dorsoventral axis (Z+=dorsal, Z-=ventral).

Specimens Requiring Additional Reconstruction

Separate from the photogrammetry derived specimen models, two specimens were obtained from other source data. Computed tomography (CT) scan data had been previously acquired for *Scaloposaurus*. The available CT data were contained in individual files containing the partial skull and axial skeleton; the tomographies had been reconstructed and partially segmented for prior study, but significant further work was necessary to completely segment all bones from the surrounding matrix and digitally articulate the skeletal model. The CT scan files were segmented in Materialise Mimics software (Materialise; Leuven, Belgium) using a combination of automated bone identification algorithms (CT Bone Wizard) and manual segmentation using simple thresholding and lasso operations to separate fossilized bone from the surrounding rock matrix. *Scaloposaurus* scan files had been previously segmented for analysis of the vertebral column; further segmentation for this study isolated right and left fore and hind limbs; pelvis; scapula; tail; skull; and partial reconstruction of the ribs. Significant disarticulation and compression of the specimen was observed; following the segmentation of individual bones, each part was exported as an STL file and imported to 3-Matic for digital repositioning of each element to its apparent in-vivo location, as well as duplication of missing or damaged body elements from the mirror side. The skull was observed by Kemp (1985) to be truncated; there is a sharp discontinuity across the snout and the most anterior aspect of the skull is absent. In order to model the full skull, an ellipsoid was modelled to represent the missing portion of the snout and scaled so that the total skull length was consistent with the estimate of Kemp (1986).

Additionally, a complete skeletal reconstruction of *Orobates pabsti* was assembled by Nyakatura et al (2015) from the holotype specimen MNG-10181. This specimen was excavated from the Bromacker quarry, (Tambach Formation, Tambach-Dietharz, Thuringia,

Germany) from a stratigraphic sequence of the lower Permian (Nyakatura et al, 2015). Due to diagenetic deformation, minor elements of specimens MNG 8980 and MNG 8966 were used to model missing or damaged components of the skeleton. The *O. pabsti* reconstruction was posed in a limb-splayed posture, with the limbs held perpendicular to the craniocaudal axis. The file was converted in Autodesk Maya (Autodesk, California, USA) from .mb file format to .OBJ and then opened in 3-Matic for rotation of the limbs into an *in vivo* posture. The model that resulted from the Nkayatura publication was made available for use through open access, and was obtained directly from the authors (personal communication).

Convex Hull and Volume Calculation Technique

After the completion of a photogrammetric or CT-derived skeletal model reconstruction, each specimen was then digitally separated into its principal body segments: skull; torso; tail; individual feet; upper and lower forelimbs; upper and lower hindlimbs; and sail (where applicable). The individual body segment object files were then run through a custom Python script that calls the *qhull* algorithm (Barber et al, 1996), generates an OBJ file of the minimum convex hull for each body segment, and calculates whole body as well as individual segment body mass and center of mass parameters from the convex hull objects (after Brassey, 2017). The individual convex hull files were then imported to Meshlab to produce visualizations and to ensure the use of realistic models of the specimens for computation (Figure 3).

Body Mass Estimation

The whole-body volume values that were generated from the convex hull procedure were then used to estimate a body mass by multiplying the body volume by an assumed density. Body segment density values from taxonomically relevant organisms in the literature

were used to provide upper and lower bounds of possible mass values. Buchner (1997) uses body segment dissection to obtain physical density values for thoroughbred horses and a total average body density of 893 kg/m^3; Cott (1961) compared the mass of a set of nine Nile crocodile on land as well as while submerged in water and computed a mean body density of 1080 kg/m^3. These two directly measured values, one from an extant mammal and one from an extant reptile, are used in this study to serve as endmember density coefficients in the body mass equation and thus yield low and high estimates of total body mass for each specimen. A "neutral" body density of 1000/kg^3, equivalent to the density of water, was also computed. The results for *L. bojani* and *T. pamelae* vary slightly from the previously published mass estimates by Romano and Rubidge (2019) and Romano and Manucci (2019) due to different methodology used here in converting volume to mass, but this was done to maintain a consistent approach with the remaining specimens in this study.

Since the convex hull routine is based only on the skeletal remains of a given species, thus yielding a minimum volume estimation, some geometric expansion of the model should be applied in order to account for fleshiness or muscle mass of the organism in its living condition as these soft tissues are not necessarily preserved in the fossil. The minimum convex hull derived body mass values were increased by a scaling factor of 21% after Sellers et al (2012) to help account for discrepancy and prevent significant underestimation of body mass. A sub-analysis was performed for *E. boanerges* and *D. milleri* by differentially applying a lower body density of 800 kg/m3 and no geometric expansion to the sail segments of each specimen, while maintaining the prior approach for the remaining body segments.

Limb Measurement Data

Limb measurements were performed to further contextualize body mass and center of mass data. Physical measurements of humerus and femur circumference were obtained from the mounted skeletal models of the initial specimen set, using a string and ruler. A total of three measurements were taken for each stylopodium, with the minimum reading being used to populate the limb scaling equations.

Additionally, digital limb measurements were performed to determine femur length. These measurements were obtained from the reconstructed photogram models in 3-Matic, using the Sketch function. This function uses a set of three points to define a 2-dimensional plane, then displays a projection of the selected three-dimensional object on that plane. For the femur measurements, 3 points were selected at the femoral head, fibular condyle, and tibial condyle; a straight line was drawn on the resultant sketch plane along the long axis of the bone in order to determine its maximal extent (figure 4).

Limb Scaling Equations

In order to provide secondary estimates of body mass, allometric limb scaling to body mass equations were used after Campione and Evans (2012). This work provides a number of line fitting equations to establish an allometric relationship between stylopodium length or circumference and body mass in tetrapods. Campione and Evans developed multiple scaling equations to produce estimates of body mass, based on different clades (mammals, reptiles, all tetrapods); separate limbs (humerus only, femur only, or both humerus and femur), and settled on a universal equation for all tetrapods based on combined humeral and femoral circumference. Since the bone length and circumferences were measured either physically or

digitally, several of these equations were used to provide a range of estimates of body mass in the sample set for this study, as well as to assess the suitability of using fitting equations from extant animals to a set of fossil specimens. A further body mass estimate was calculated using the stylopodium measurements in a quadratic form curve fitting equation derived from Campione (2017), as there has been some question as to whether the limb dimension and body mass relationship is truly linear across all body size regimes.

Stylopod robustness was estimated for the fossil dataset as well as the extant tetrapod dataset from Campione and Evans (2012), defined as a ratio of humerus and femur circumference to length (C/L). The data ranges for each taxon were compared using a one-way ANOVA in RStudio using the *aov* function in order to assess significance of any observed difference between these groups.

Confidence intervals for body mass estimates from both volumetric density and limb scaling approaches were determined from the literature. The universal limb scaling equation of Campione & Evans (2012) gives a mean percent predictive error range of 25.6%, which was used to create lower and upper bounds around the point estimate given by solving the equation. For the volumetric density approach modeled after Sellers et al (2012), the expansion constant defined by the slope of the regression line is given as 1.206, while the 95% confidence interval is defined as 1.091-1.322; these are used as the upper and lower bounds of the volumetric estimates.

Center of Mass Calculations

The center of mass coordinates for each specimen (total body as well as each individual body segment) were calculated in the Python script concurrent to body volume

calculation. Each center of mass output value is a coordinate set representing the center of mass in Cartesian space with respect to the origin.

The output values were normalized to permit comparison between specimens of different size by computing the position of the center of mass as a ratio of the distance from the acetabulum to the glenoid. The locations of the acetabulum and glenoid were determined visually from the model by placing a digital marker or line through each socket and determining its three-dimensional coordinate. The coordinate values for center of mass, glenoid position, and acetabulum position were then considered as the vertices of a triangle. Each side length of the triangle was calculated using the equation

$$\sqrt{[(X_1-X_2)^2+(Y_1-Y_2)^2+(Z_1-Z_2)^2)]};$$

where each (X, Y, Z) triplet represents one of the vertices. The area of the triangle was calculated using Hero's formula:

$$Area=\sqrt{[s*(s-a)*(s-b)*(s-c)]};$$

Where s is the semi-perimeter of the triangle, and a, b, and c are the side lengths of the triangle. The height of the triangle was subsequently calculated using the formula

$$h=2 \times Area/base;$$

where the base of the triangle is defined as the line from the glenoid to the acetabulum (Figure 5).

The height therefore represents a line segment originating from the center of mass location, that bisects the line from the glenoid to the acetabulum. The location of that intersection is used to determine the relative cranial or caudal position of the center of mass along the glenoid-acetabulum axis, by calculating a right triangle with sides represented by the height

calculated in the last step (h; figure 5); the line between the center of mass and the acetabulum position (side AC; figure 6); and the line from the intersection of the height and the glenoid-acetabulum axis with the location of the acetabulum (segment DC; Figure 5). The height and the side AC are known and can be used to calculate the length of DC using Pythagoras's theorem; segment BD can then be determined by inference. The ratio of BD:BC expresses the center of mass as a fraction cranial from the acetabulum to the glenoid (Figure 6).

In order to assess the effect of individual body segments on the results, the normalized center of mass was compared to the relative skull and tail mass ratio, defined by:

$$\ln(\text{volume}_{\text{skull}}/\text{volume}_{\text{tail}})$$

To ensure that the relationship in this linear model is not impacted by phylogenetic similarity of different specimens, the phylogenetic independent contrast method (PIC) was applied to this regression in RStudio using the *ape* library and the *phytools* package (Revell, 2012). A composite tree of 8 species (excluding *O. pabsti*) was constructed by pruning time-scaled master phylogenies of fossil synapsids and tetrapods from Jones *et al,* 2019 and Dickson *et al*, 2020, respectively. For *O. pabsti*, age and divergence from *D. tenuitectes* were sourced from Kissel 2010. The final ultrametric composite phylogeny was generated using Mesquite v3.61 and the 'ape' package in R (R Core Team, 2020).

III. Results

Body Mass Results

A total of 9 different body mass estimate ranges were calculated for each specimen (Figure 7). The smallest specimen, *Scaloposaurus*, has a mass estimate range from 0.11-1.35 kg; the largest specimen, *Lisowicia,* gives an estimate range of 5018-13202 kg. The results for *L. bojani* and *T. pamelae* are consistent with the published "average model" mass estimates by Romano and Rubidge (2019) and Romano and Manucci (2019): the volumetric estimates for *L. bojani* here range from 5018-6800 kg for varying density, compared to 5043-5860 kg; for *T. pamelae*, volumetric body mass estimates range from 785-1063 kg compared to a published range of 791-1010 kg. Similarly, the digital model of *O. pabsti* was given a body mass estimate range of 2.75-5.21 kg (mean 3.98 kg) by Nyakatura *et al* (2015); using the neutral density and 21% expansion approach in this study gives an estimate range of 3.85-4.67 kg (mean 4.27 kg) from the same model. The sub-analysis of the two sail-backed pelycosaurs yielded a new body mass estimate of 41.5 kg for *D. milleri* and 98.2 kg for *E. boanerges*, reducing the overall size by around 7% in each model.

Comparison of Volumetric and Scaling Equation Estimates

In 9 of 11 specimens, volumetric estimates of body mass were consistently below the lower bound of the 95% confidence intervals suggested by the limb scaling equations derived from Campione and Evans (2012, 2017). In one specimen (*D. milleri*) volumetric results were below mean limb scaling estimates but within the 95% CI; in another specimen (*E. Boanerges*) volumetric estimates were higher than limb scaling but within 95% CI (Figure 7). Of the 9 specimens which show significantly higher body mass estimate results from the

universal limb scaling method, the amount of overestimation ranges from 47% to 352% when compared to volumetric density models based on neutral density and 21% expansion. The results from an ANOVA performed on limb bone robustness indicate that the fossil taxa in this study have significantly more robust humeri ($p = 0.0009$) and femora ($p = 0.00005$) than both extant mammals and extant reptiles.

Center of Mass Results

Center of mass results are presented here as a coordinate set giving the distance, in mm, from the origin of the three-dimensional space, (0, 0, 0). Results are given for both the reference pose and the limb-splayed pose, with limbs held perpendicular to the body (Table 4). Minor differences in total body center of mass results were observed between the two postures; an average caudal shift of 0.34% in the limb-splayed pose was computed with a range of 3.3% to (-2.98%). Center of mass coordinates are also given for each individual body segment (table 6).

The whole-body center of mass position is normalized in two ways to account for variation in body size (Table 5). First, the center of mass is expressed as a fraction of the distance from the acetabulum to the glenoid. The results range from 40%-75% cranial from the acetabulum; the most cranial COM position is *S. punctatus*, while the most caudally positioned COM is *E. boanerges*. Outside of *S. punctatus*, which presents certain evidence of juvenile form, the normalized results are more constrained, between 40-60% cranial from the acetabulum (Figure 8).

A clear relationship was observed between a large skull/tail ratio and a more anterior center of mass location (R^2: 0.8684; $p= 0.00016$) (Figure 9a). After the PIC correction, the fit

statistics show that the linear relationship between skull:tail mass ratio and center of mass position was still observed (R^2: 0.9035, p= 0.00005), (Figure 9b).

Center of mass has also been normalized by dividing the distance from COM to the acetabulum by the length of the femur, with both measurements in mm (Table 5). The resultant values range from a minimum of 1.42 in *D. tenuitectes* to a maximum of 2.11 in *O. uniformis*; in other words, all specimens show that the center of mass is greater than 1 femur length cranial from the acetabulum (Figure 9).

IV. Discussion

Body Mass Estimations

Throughout the series of pre-mammalian tetrapods that comprise the sample dataset, a great range of body mass values were observed with four orders of magnitude between the smallest (## g) and largest specimens (## kg). This is unsurprising, as the specimen set covers a lineage with significant phylogenetic diversity and breadth. Furthermore, while the species contained in this study represent an evolutionary grade of families from Anamniotes up until Therapsids, each family is represented by only a single specimen, in no way representing the physiological diversity that is known to be present in each group. Still, there is a trend of increasing body size, likely associated with herbivory, in the transition from the earliest synapsids of the Carboniferous to the enormous dicynodont therapsids of the Permian in *D. turpior and L. bojani,* and a marked decrease in body size in the later therocephalian *Scaloposaurus* and the early cynodont *Procynosuchus*. These observations are consistent with prior analyses of body size in the non-mammalian synapsids and therapsids (Huttenlocker 2014; Brocklehurst & Brink, 2017; Reisz & Frobisch, 2014; Brocklehurst, 2019). Later therapsids, and the earliest Mesozoic mammals in the Triassic and Jurassic have been estimated to have even smaller body size, including many early mammals smaller than 0.1 kg (Slater, 2013).

Are Volumetric Models Missing Mass?

There is a clear trend of volumetric model ranges estimating smaller mass than linear or quadratic model bone scaling estimates, both in the literature and in this study (Bates et al 2015; Brassey et al 2015; Romano and Manucci, 2019). While there is no ground truth value to provide the “correct” answer when discussing fossil taxa since measurements can’t be

taken directly, it is worth assessing both models to determine where they may be over- or underestimating mass. In the case of the volumetric density model, there are very few input parameters that can account for "missing" mass: either the volume is too small, or the density used is too low. It is known that a minimum convex hull used to simulate individual body segments is tightly bounded to the bone underneath and will underestimate volume of soft tissue; this has been accounted for by applying the 21% arithmetic expansion of the volume after Sellers (2012). Similarly, in the therapsid reconstructions by Romano & Rubidge (2019) and Romano & Manucci (2019), the analysis included the creation of "slim," "average," and "fat" models based on the degree of modeling of soft tissue to be added to the skeletal reconstruction. Based on these reconstruction efforts, for *T. pamelae* the fat model was approximately 28% larger by volume than the slim model, while for *L. bojani* the increase was around 24%. These values taken in conjunction with the Sellers *et al.* equation suggest that the constraint for the amount of underestimation based on the minimum convex hull method is around 20-30%.

It is worth noting that there are two specimens which do not show significant disagreement between the volumetric density estimates and the limb scaling method, and both are "pelycosaurs" with large dorsal sails; this raises the possibility that the effect of these sails are somehow skewing the volumetric body mass estimate higher. An overestimation of mass from a volumetric body segment will be predicated on two possibilities: the volume of the convex hull is larger than the body segment in the living organism, or the density of the segment is too high (Figure 3). The large dorsal sails are somewhat unusual features, not present in all fossil taxa studied, and they may yield body segment mass estimates that are too high when applying the same 21% expansion and 1000 kg/m3 density as the rest of the body segments. Romer and Price (1940) note that the sail of

Dimetrodon was comprised of "slender spines and large skin webs between." The convex hull for the sail segment is based on the bones which were preserved; since there were not significant amounts of soft mass or musculature in the living organism, the convex hull likely represents an accurate representation of the sail geometry without needing the 21% increase following Sellers. These could still be overestimating sail volume, and further work may be needed to investigate the appropriate segment density from modern specimens as well. However, given that the sails represent around 10-12% of the total body volume of each specimen there is a lower limit to how much total effect adjusting the parameters of the sail can have on the total mass.

It is also important to consider the extent to which any synapsid-specific morphology may not be reflected in the fossil record. For example, many volumetric reconstruction estimates are based on the calibration curve of Sellers *et al.* (2012) which was developed based on extant mammals. While the synapsids studied here are considered mammalian forerunners, there are certain physical characteristics that did not appear until the evolution of mammals, and which could cause an underestimation of body volume due to differences in fossil preservation. Some early synapsids are known to have partially cartilaginous ribs which may not be preserved, yielding an incomplete and therefore uncertain rib morphology as the convex hull will not model any soft tissue that would hang below the lower bound of the ribcage (Janis & Keller, 2001). Many modern and extinct reptiles have separated abdominal ribs or gastralia which hang below the extent of the dorsal rib cage, and similar observations have been made in varanopid synapsids (Botha-Brink 2007; Maddin, *et al* 2020). While this is a possible source of body mass underestimation, the average body mass increase to the volumetric model that is needed to bring the 95% confidence intervals to overlap with the limb scaling method is 59%, which is much too large to simply be missing soft mass from the

gut. In Figure 11, the volumetric reconstruction of *D. turpior* shows the minimum, "shrink-wrapped" convex hull (a); a 21% volume expansion after Sellers *et al* (2012) (b); and a 352% increase needed to attain a volume where a neutral density would give a mass equivalent to the combined stylopodial circumference universal limb scaling equation (c).

Is There Something About the Synapsid Stylopodia?

An alternative hypothesis to explain the discrepancy between estimation methods would suggest that applying the universal limb scaling equation is significantly overestimating body mass. Just as with volumetric mass estimates, limb scaling equations are unable to be calibrated based on fossil taxa and are thus describing a length-mass relationship specific to modern animals. The stylopodia are utilized to estimate mass in a biomechanical context, as these bones must support the full weight of the organism during locomotion (Campione, 2020). Using a calibration curve derived from modern specimens and applying it to fossil limb bones assumes that the constraints limiting the morphology of extant tetrapod limbs are identical to animals that have been walking around on this planet for hundreds of millions of years. It has been noted by others that the large bodied non-mammalian synapsids and therapsids had very robust limb bones associated with their sprawling posture; in their reconstruction of *Lisowicia*, Romano and Manucci (2019) observe that the femur bone is so robust that, in order to scale an extant elephant femur to match the axial circumference of *Lisowicia*, the resulting elephant would stand 15 meters tall.

Sprawling limb posture involves mechanical stress on the limbs with significant torsional loading on the humerus and femur (Blob, 2001; Biewener,1990). Upright or parasagittal postures, which are associated with most modern mammals and large bodied animals, reduce

this torsional stress by aligning the limb bones to the vector of the ground reaction force (Blob 2001). Given the increased torsional stress on long bones, the mechanical strength of the humerus and femur for a given body mass should be increased in sprawling taxa when compared to upright taxa in order to maintain sufficient safety factors in response to mechanical stresses applied to the limbs during locomotion. While the use of simple linear measurements does not account for any variability in strength due to bone cross sectional symmetry, analysis of the calibration dataset used by Campione and Evans shows modest increase in stylopod "robustness" as defined by measuring humerus or femur circumference divided by length [C_h/L_h; C_f/L_f] in extant reptiles. However, analysis of variance of the fossil taxa measured in this study show significantly higher values of both femur ($F(1,229)=16.89$; $p=0.00005$) and humerus ($F(1,249)=11.28$; $p=0.0009$) robustness compared to both extant reptiles and mammals, suggesting that there are significant morphological differences between the limb bone design of the fossil taxa studied when compared to the extant mammals and reptiles used to generate the universal limb scaling equation. (Figure 12). While the limb scaling dataset does include modern reptiles, which exhibit sprawling limb posture, there is a limitation due to the relative lack of large, sprawling organisms among modern taxa. The limb scaling dataset includes only 6 reptiles which have a measured body mass larger than 5 kg; of those, at least 3 are semi-aquatic which might indicate limb morphologies that are suited to different types of stress than terrestrial tetrapods. Since 8 of the 11 specimens in this study have body size larger than 5 kg and sprawling posture, it seems that there may be a fundamental issue with estimating body mass based on limb circumference.

Factors Influencing Center of Mass Position

Center of mass (COM) estimations are highly variable between species; COM values are given as coordinate location in three-dimensional cartesian space and are highly dependent on the total body size of the animal, as craniocaudal axis coordinate values vary by an order of magnitude. For center of mass position normalized as a fraction of the distance from the acetabulum and the glenoid fossae, the normalized values are constrained within a range of approximately 0.4-0.6 (indicating that the center of mass is positioned 40-60% cranial along the line connecting the acetabulum and glenoid), with the exception of *Scaloposaurus*, which gives a normalized value of 0.75.

This is notable as multiple researchers have suggested that *Scaloposaurus* may be a catch-all taxon for juvenile specimens of other therocephalian; these assessments have been made based on various aspects of cranial morphology, dentition, or lack of ossification or periosteal bone in the postcranial skeleton (Kemp, 1986; Huttenlocker, 2009; Huttenlocker & Sidor, 2012). An extremely anterior center of mass position with respect to the rest of the dataset may be consistent with the proposed juvenile status. Otero *et al* (2019) hypothesized that ontogenetic development in *Mussaurus patagonicus* was associated with a continued caudal shift in center of mass. Allen *et al* (2009), found that development in crocodylians was associated with a cranial shift in COM, and hypothesized that throughout their ontogeny most archosaurs develop more robust heads and relatively shortening limbs. Young and Shapiro (2018) state that in primate mammals, ontogeny is associated with a caudal shift in center of mass position marked by a relative decrease in head mass as a total of body size and an increase in limb and trunk dimensions. *Scaloposaurus,* a therocephalian therapsid, shares a number of derived characteristics with mammals, it would be reasonable to consider an ontogenetic track more similar to that of mammals than of archosaurs.

The results from normalization with respect to femur length are consistent with the prior hypotheses of Otero et al (2019) and Allen et al (2009) that a value of less than 1 permits static stability in the bipedal posture, as all of the specimens studied here are expected to be obligate quadrupeds (figure 9).

Effect of Individual Body Segment on Center of Mass

In addition to *Scaloposaurus*, many of the non-mammalian synapsids and therapsids display disparate morphological characteristics which have an overall effect on the calculated center of mass location. From Figure 9, it is evident that the relative size of an animal's head and tail have a significant impact on the position of the total body center of mass, with a higher skull to tail index resulting in a more cranial center of mass positioning. An extreme example, *E. boanerges*, has a very small head, a large, barrel shaped trunk segment, and a long, heavy tail; its center of mass is the most caudally positioned in the sample set. In contrast, *D. milleri* displays a larger skull despite smaller overall body size and a smaller tail; the center of mass is positioned more cranially. To contextualize this in terms of gait, *E. boanerges* had longer, more massive forelimbs than hindlimbs, which may have been necessary to drag its large body. Further work would be necessary to investigate the extent to which center of mass position is related to limb musculature and its implications for locomotion.

Center of mass can also be analyzed in this dataset in an evolutionary context. While whole body data on modern quadrupedal mammals are scarce, a recent analysis found that primates, which are capable of multiple modes of locomotion, display total body center of mass of between 40-60% when normalized to the hip-shoulder distance as done in this study (Druelle *et al*, 2019). This is surprisingly similar to the results found here, given the significant differences in morphological characteristics and ecological habits between study

groups. The same study also observed a center of mass range of approximately 50-65% within a small subset of quadrupedal mammals. Further analyses of both modern quadrupedal mammals as well as early Mammaliaforms would help to determine whether these constraints for center of mass position have shifted significantly throughout the synapsid lineage.

Limitations and Future Directions

Principal limitations to this study are driven by the relatively small size of the specimen set; future work should look to developing volumetric reconstructions for more species, especially later cynodont therapsids and early mammaliaforms, in order to gain further insight into the history of body size evolution in the synapsid lineage leading to mammals. Individual body segment density values may be an important line of inquiry for improving the accuracy of volumetric reconstructions, with particular attention for this group on understanding the volume and density of the dorsal sail. Incorporating further specimens will also increase the understanding on the center of mass constraints in terrestrial quadrupeds. Additionally, center of mass results can be further contextualized based on the influence of individual body segments beyond the skull and tail, by investigating segment inertial parameters including first mass moments.

Conclusions

The evolutionary history of synapsids leading to mammals includes a wide range of body sizes and morphological characteristics. This study compared multiple methods for estimating body mass and center of mass position for a diverse group of species that span this transition. Within this group, body mass estimates that are based on volumetric reconstructions may be preferable due to the significant differences in stylopod morphology when compared against the extant taxa used to derive the limb scaling equations. The body

mass results are consistent with the expectation of a gradual increase throughout the synapsid lineage to the therapsid grade, followed by a dramatic reduction in body size prior to the evolution of mammals. In addition, center of mass results are seen here to be constrained among tetrapods within a range 40-60% from the hip to the shoulder, combining the data from this study with the literature. The specimens digitized here show that these results are significantly influenced by variations in skull and tail dimension.

References

Ahlberg, P.E., Clack, J. A, & Blom, H. (2005). The axial skeleton of the Devonian tetrapod Ichthyostega. Nature, 437(7055), 137-140.

Allen, V., Paxton, H., and Hutchinson, J. (2009). Variation in Center of Mass Estimates for Extant Sauropsids and its Importance for Reconstructing Inertial Properties of Extinct Archosaurs. The Anatomical Record. 292:1442–1461.

Barber, C.B., Dobkin, D.P., and Huhdanpaa, H.T., "The Quickhull algorithm for convex hulls," ACM Trans. on Mathematical Software, 22(4):469-483, Dec 1996, http://www.qhull.org.

Basu, C., Falkingham, P., and Hutchinson, J. (2016). The extinct, giant giraffid Sivatherium giganteum: skeletal reconstruction and body mass estimation. 12.Biol. Lett.

Bates, K., Falkingham, P., Macaulay, S., Brassey, C., & Maidment, S. (2015). Downsizing a giant: Re-evaluating Dreadnoughtus body mass. Biology Letters, 11(6), 20150215.

Benton, M. J. (2009). Vertebrate palaeontology, 3rd edition (3rd ed.). Wiley.

Biewener, A.A. (1990). Biomechanics of Mammalian Terrestrial Locomotion. Science (American Association for the Advancement of Science), 250(4984), 1097-1103.

Blob, R. (2001). Evolution of hindlimb posture in nonmammalian therapsids: Biomechanical tests of paleontological hypotheses. Paleobiology, 27(1), 14-38.

Botha-Brink, J., & Modesto, S.P. (2007). A mixed-age classed 'pelycosaur' aggregation from South Africa: Earliest evidence of parental care in amniotes? *Proceedings of the Royal Society. B, Biological Sciences, 274*(1627), 2829-2834.

Brassey, C.A., & Sellers, W. I. (2014). Scaling of convex hull volume to body mass in modern primates, non-primate mammals and birds. PLoS ONE, 9(3), E91691.

Brassey, C., Maidment, S., and Barrett, P. (2015). Body mass estimates of an exceptionally complete Stegosaurus (Ornithischia: Thyreophora): comparing volumetric and linear bivariate mass estimation methods. Biol. Lett.11:20140984.

Brocklehurst, Neil, & Brink, Kirstin S. (2017). Selection towards larger body size in both herbivorous and carnivorous synapsids during the Carboniferous. Facets (Ottawa), 2(1), 68-84.

Brocklehurst, N. (2019). Morphological evolution in therocephalians breaks the hypercarnivore ratchet. Proceedings of the Royal Society. B, Biological Sciences, 286(1900), 20190590.

Buchner, H.H.F, Savelberg, H.H.C.M, Schamhardt, H.C, & Barneveld, A. (1997). Inertial properties of Dutch Warmblood horses. Journal of Biomechanics, 30(6), 653-658.

Campione, Nicolás E, & Evans, David C. (2012). A universal scaling relationship between body mass and proximal limb bone dimensions in quadrupedal terrestrial tetrapods. BMC Biology, 10(1), 60.

Campione, Nicolás E. (2017). Extrapolating body masses in large terrestrial vertebrates. Paleobiology, 43(4), 693-699.

Campione, Nicolás E, & Evans, David C. (2020). The accuracy and precision of body mass estimation in non-avian dinosaurs. Biological Reviews of the Cambridge Philosophical Society, 95(6), 1759-1797.

Cott, H. (1961). Scientific results of an inquiry into the ecology and economic status of the Nile Crocodile (Crocodilus niloticus) in Uganda and Northern Rhodesia (Zoological Society of London. Transactions; v. 29). London: Zoological Society of London.

De Oliveira, T.V., & Schultz, C.L. (2016). Functional morphology and biomechanics of the cynodont Trucidocynodon riograndensis from the triassic of Southern Brazil: Pectoral girdle and forelimb. Acta Palaeontologica Polonica, 61(2), 377-386.

Dickson, B.V., Clack, J.A., Smithson, T.R. et al. Functional adaptive landscapes predict terrestrial capacity at the origin of limbs. Nature 589, 242–245 (2021).

Druelle, F., Berthet, M., & Quintard, B.. (2019). The body center of mass in primates: Is it more caudal than in other quadrupedal mammals? American Journal of Physical Anthropology, 169(1), 170-178.

Huttenlocker, A. (2009). An investigation into the cladistic relationships and monophyly of therocephalian therapsids (Amniota: Synapsida). Zoological Journal of the Linnean Society, 157(4), 865-891.

Huttenlocker, A.K., & Sidor, C.A. (2012). Taxonomic Revision of Therocephalians (Therapsida: Theriodontia) from the Lower Triassic of Antarctica. American Museum Novitates, 3738(3738), 1-19.

Huttenlocker, A. K. (2014). Body size reductions in nonmammalian eutheriodont therapsids (Synapsida) during the end-Permian mass extinction. PloS One, 9(2), E87553.

Janis, C.M., and Keller, J.C. (2001). Modes of ventilation in early tetrapods: Costal aspiration as a key feature of amniotes. Acta Palaeontologica Polonica 46 (2), 2001: 137-170

Jones, K. E., K.D. Angielczyk, and S.E. Pierce. “Stepwise shifts underlie evolutionary trends in morphological complexity of the mammalian vertebral column.” Nature Communications 10, no. 5071 (2019): 1-13.

Kemp, T. (2005). The origin and evolution of mammals. Oxford; New York: Oxford University Press.

Luo, Z.X. (2007). Transformation and diversification in early mammal evolution. Nature (London), 450(7172), 1011-1019.

Mallison, H. (2010). The Digital Plateosaurus I: Body Mass, Mass Distribution and Posture Assessed Using CAD and CAE on a Digitally Mounted Complete Skeleton. Palaeontologia Electronica Vol. 13, Issue 2; 8A: 26p.

Maddin, H. C., Mann, A., & Hebert, B. (2020). Varanopid from the Carboniferous of Nova Scotia reveals evidence of parental care in amniotes. Nature Ecology & Evolution, 4(1), 50-56.

Mann, A., & Paterson, R. S. (2020). Cranial osteology and systematics of the enigmatic early 'sail-backed' synapsid Echinerpeton intermedium Reisz, 1972, and a review of the earliest 'pelycosaurs'. Journal of Systematic Palaeontology, 18(6), 529-539.

Nyakatura, J.A., Allen, V.R., Lauströer, J., Andikfar, A., Danczak, M., Ullrich, H.J., Fischer, M.S. (2015). A Three-Dimensional Skeletal Reconstruction of the Stem Amniote Orobates pabsti (Diadectidae): Analyses of Body Mass, Centre of Mass Position, and Joint Mobility. PLoS ONE, 10(9), E0137284.

Otero, A., Cuff, A., Allen, V., Sumner-Rooney, L., Pol, D., & Hutchinson, J. (2019). Ontogenetic changes in the body plan of the sauropodomorph dinosaur Mussaurus patagonicus reveal shifts of locomotor stance during growth. Scientific Reports, 9(1), 7614.

Pierce, S. E., Clack, J. A., & Huthcinson, J. R. (2012). Three-dimensional limb joint mobility in the early tetrapod Ichthyostega. Nature (London), 486(7404), 523-526.

Regnault, Sophie, Fahn-Lai, Philip, Norris, Rachel M, & Pierce, Stephanie E. (2020). Shoulder Muscle Architecture in the Echidna (Monotremata: Tachyglossus aculeatus) Indicates Conserved Functional Properties. Journal of Mammalian Evolution, 27(4), 591-603.

Reisz, Robert R, & Fröbisch, Jörg. (2014). The oldest caseid synapsid from the Late Pennsylvanian of Kansas, and the evolution of herbivory in terrestrial vertebrates. PloS One, 9(4), E94518.

Revell LJ (2012). “phytools: An R package for phylogenetic comparative biology (and other things).” *Methods in Ecology and Evolution*, **3**, 217-223.

Romano, Marco, & Rubidge, Bruce. (2019). First 3D reconstruction and volumetric body mass estimate of the tapinocephalid dinocephalian Tapinocaninus pamelae (Synapsida: Therapsida). Historical Biology, 1-8.

Romano, Marco, & Manucci, Fabio. (2019). Resizing Lisowicia bojani: Volumetric body mass estimate and 3D reconstruction of the giant Late Triassic dicynodont. Historical Biology, 1-6.

Romer, A. and Price, L. (1940). Review of the Pelycosauria. Geological Society of America Special Papers, Vol. 28.

Schmidt-Nielsen, K. (1984). Scaling, why is animal size so important? Cambridge [Cambridgeshire]; New York: Cambridge University Press.

Sellers, Hepworth-Bell, Falkingham, Bates, Brassey, Egerton, & Manning. (2012). Minimum convex hull mass estimations of complete mounted skeletons. Biology Letters, 8(5), 842-845.

Young, J. W, & Shapiro, L. J. (2018). Developments in development: What have we learned from primate locomotor ontogeny? American Journal of Physical Anthropology, 165, 37-71.

Appendix

Figures and Tables

Table 1. List of selected specimens for this study. Museum abbreviations are as follows: Museum of Comparative Zoology, Harvard (MCZ); National Museum, Bloemfontein (NMQR); Institute of Paleobiology, Polish Academy of Sciences (ZPAL); University Museum of Zoology, Cambridge (UMZC); Collection of Tom Kemp (TSK).

Species	Collections #	Period	Formation	Locality
Eryops megacephalus	MCZ VPRA-1539	Lower Permian	Belle Plains fm.	Baylor County, TX
Orobates pabsti	MNG 10181 (elements MNG 8980 and MNG 8966)	Lower Permian	Tambach fm.	Tambach-Dietharz, Thuringia
Diadectes tenuitectes	MCZ VPRA-1035	Lower Permian	Admiral fm.	Baylor County, TX
Ophiacodon uniformis	MCZ VPRA-1366	Lower Permian	Putnam fm.	Archer City, TX
Edaphosaurus boanerges	MCZ VPRA-1531 and 1764	Lower Permian	Admiral fm.	Archer County, TX
Dimetrodon milleri	MCZ VPRA-1365	Lower Permian	Putnam fm.	Archer City, TX
Tapinocaninus pamelae	NMQR 2987	Middle Permian	Abrahamskraal fm, Beaufort Group	Prince Albert district, Western Cape, South Africa
Dinodontosaurus turpior	MCZ VPRA-1670	Triassic	Santa Maria Supersequence	Rio Grande do Sul, Brazil
Lisowicia bojani	Multiple specimens; Institute of Paleobiology, ZPAL	Late Triassic	Lipie Śląskie	Lisowice, Poland
Scaloposaurus punctatus	UMZC T837	Lower Triassic	*Lystrosaurus* zone	South Africa
Procynosuchus delaharpeae	TSK 34*	Upper Permian	Madumabisa Mudstones	Middle Luangwa Valley,Zambia

Table 2. Mass estimates using the volumetric reconstruction approach. Minimum density = 893 kg/m3; maximum density = 1080 kg/m3. 21% expansion based off of Sellers et al (2012).

Specimen	Convex Hull Volume (m^3)	Minimum Density Body Mass Estimate (kg)	Maximum Density Body Mass Estimate (kg)	Body Mass, Neutral Density + 21% Expansion (kg)
Eryops megacephalus	0.073	65.37	79.06	74.74
Orobates pabsti	0.0035	3.15	3.81	3.60
Diadectes tenuitectes	0.1143	102.07	123.44	116.70
Ophiacodon uniformis	0.0186	16.61	20.09	18.99
Edaphosaurus boanerges	0.0872	77.87	94.18	89.03
Dimetrodon milleri	0.0366	32.68	39.53	37.37
Dinodontosaurus turpior	0.2191	195.66	236.63	223.70
Scaloposaurus punctatus	0.0003	0.245	0.30	0.28
Procynosuchus delaharpeae	0.0029	2.55	3.09	2.92
Tapinocaninus pamelae	0.879	784.95	949.32	897.46
Lisowicia bojani	5.62	5018.66	6069.60	5738.02

Table 3. Stylopod measurements and limb scaling equation body mass estimate results. Asterisk (*) indicates limb measurements taken digitally. C_{H+F} based on the universal scaling equation from combined humerus and femur circumference (Campione & Evans, 2012).

	* denotes digital measurement		Body Mass Estimates after Campione & Evans, 2015; Campione, 2017); kg			
Specimen	Humerus circumference (mm)	Femur circumference (mm)	C_{H+F} model	C_H model	C_F model	Quadratic Model
Eryops megacephalus	113.00	122.67	244.56	225.79	294.46	239.89
Orobates pabsti	30.32*	50.26*	13.68	6.90	23.83	13.93
Diadectes tenuitectes	141.67	157.67	471.34	411.16	597.35	455.50
Ophiacodon uniformis	53.33	61.00	33.01	30.85	41.12	33.38
Edaphosaurus boanerges	62.67	80.67	61.26	47.31	90.38	61.52
Dimetrodon milleri	62.67	63.67	44.75	47.31	46.39	45.12
Dinodontosaurus turpior	232.67	182.33	1198.24	1531.84	899.75	1128.92
Scaloposaurus punctatus	12.69*	12.64 *	1.10	1.14	2.85	1.11
Procynosuchus delaharpeae	32.7*	30.09*	6.89	8.43	5.61	7.03
Tapinocaninus pamelae	250	237	1923.17	1853.27	1883.83	1785.37
Lisowicia bojani	410	455	9329.48	6878.44	11837.94	8169.98

Table 4. Center of mass coordinates derived from both a reference pose and a limb splayed pose. Reference pose indicates the life pose of mounted specimens; limb splayed pose holds limbs horizontally away from the body.

Specimen	Reference Pose Center of Mass Coordinate			Limb Splayed Pose Center of Mass Coordinate		
	X	Y	Z	X	Y	Z
Ophiacodon uniformis	-9.26	-578.05	-68.63	-6.40	-588.21	-67.76
Dimetrodon milleri	2.87	-554.57	-39.31	-1.17	-582.19	-44.12
Edaphosaurus boanerges	-16.852	-725.31	-12.18	-2.52	-734.85	30.64
Eryops megacephalus	11.61	-710.56	-46.37	12.09	-711.81	-41.99
Diadectes tenuitectes	-7.044	-831.44	-62.24	1.76	-806.68	-82.18
Dinodontosaurus turpior	-19.28	-903.64	-14.54	-16.46	-883.73	11.97
Procynosuchus delaharpeae	13.73	-317.25	-75.53	7.18	-318.26	-73.84
Orobates pabsti	-3.77	-324.53	-20.97	-2.04	-324.42	-15.20
Scaloposaurus punctatus	-4.26	-106.13	-15.81	-4.18	-106.42	-13.83

Table 5. Center of mass position relative to acetabulum-glenoid transect and length of the femur.

Specimen	CoM% Cranial to Acetabulum	Femur length (mm)	Distance CoM to Acetabulum (mm)	COM-Acetabulum/Femur Length
Eryops megacephalus	59.5%	189.86	322.87	1.70
Orobates pabsti	51.3%	82.48	141.82	1.72
Diadectes tenuitectes	45.3%	221.46	322.84	1.46
Ophiacodon uniformis	53.1%	117.29	247.09	2.11
Edaphosaurus boanerges	44.6%	163.25	338.90	2.08
Dimetrodon milleri	56.7%	149.29	305.30	2.04
Dinodontosaurus turpior	60.3%	323.60	497.08	1.54
Scalaposaurus punctatus	74.8%	38.00	69.16	1.82
Procynosuchus delaharpae	55.9%	77.53	151.20	1.95

Table 6. Individual Body Segment Volume, Density, and Center of Mass Estimates. All models here used a density of 1000 kg/m3.

Specimen, Pose	Segment Name	Volume (mm3)	Segment COM X	Segment COM Y	Segment COM Z	Segment Mass (g)	Segment Mass (kg)
Eryops Megacephalus Reference Pose	Skull	12937.98	6.21	-263.72	16.07	12937.98	12.94
	Right hindlimb upper	442.02	190.71	-998.09	-152.09	442.02	0.44
	Right hindlimb lower	584.85	255.75	-995.77	-199.03	584.85	0.58
	Right hindlimb foot	304.24	300.97	-965.96	-275.47	304.24	0.30
	Left hindlimb upper	583.95	-167.92	-1018.43	-150.67	583.95	0.58
	Left hindlimb lower	560.80	-246.45	-1008.42	-200.70	560.80	0.56
	Left hindlimb foot	302.81	-292.19	-977.61	-272.64	302.81	0.30
	Tail	1765.42	17.74	-1372.14	-105.95	1765.42	1.77
	Tail b	335.44	14.41	-1619.76	-194.41	335.44	0.34
	Torso	52820.42	12.99	-785.62	-45.29	52820.42	52.82
	Right forelimb upper	397.35	180.26	-491.80	-164.55	397.35	0.40
	Right forelimb lower	428.47	246.35	-468.89	-217.98	428.47	0.43
	Right forelimb foot	115.72	223.68	-376.43	-259.11	115.72	0.12
	Left forelimb upper	385.92	-152.68	-488.47	-168.83	385.92	0.39
	Left forelimb lower	377.19	-212.73	-459.56	-224.20	377.19	0.38
	Left forelimb foot	135.40	-188.27	-370.17	-260.08	135.40	0.14
Eryops Megacephalus Limb Splayed Pose	Skull	12937.98	6.21	-263.72	16.07	12937.98	12.94
	Right hindlimb upper	442.02	191.20	-1030.64	-113.67	442.02	0.44
	Right hindlimb lower	584.85	329.94	-1037.57	-133.00	584.85	0.58
	Right hindlimb foot	304.24	432.07	-1053.78	-141.32	304.24	0.30
	Left hindlimb upper	583.95	-166.70	-1032.03	-107.31	583.95	0.58
	Left hindlimb lower	560.79	-321.55	-1022.60	-100.24	560.79	0.56
	Left hindlimb foot	302.81	-429.96	-1023.50	-86.14	302.81	0.30
	Tail	1765.42	17.74	-1372.14	-105.95	1765.42	1.77
	Tail b	335.44	14.41	-1619.76	-194.41	335.44	0.34

	Torso	53225.37	13.55	-784.14	-46.19	53225.37	53.23
	Right forelimb upper	397.35	188.77	-478.79	-129.25	397.35	0.40
	Right forelimb lower	428.47	289.06	-481.35	-145.12	428.47	0.43
	Right forelimb foot	115.73	392.39	-463.13	-142.49	115.73	0.12
	Left forelimb upper	385.92	-153.09	-494.76	-114.65	385.92	0.39
	Left forelimb lower	377.19	-253.01	-502.47	-133.78	377.19	0.38
	Left forelimb foot	135.40	-351.99	-486.36	-124.45	135.40	0.14
Orobates Pabsti Reference Pose	Skull	254.40	-2.20	-72.34	-2.51	254.40	0.25
	Tail	220.85	-1.27	-611.95	-7.63	220.85	0.22
	Torso	2401.06	-1.35	-315.88	-13.83	2401.06	2.40
	Left forelimb upper	53.95	-61.36	-199.76	-42.97	53.95	0.05
	Right forelimb upper	53.95	61.36	-199.76	-42.97	53.95	0.05
	Left forelimb lower	21.61	-95.36	-188.58	-64.72	21.61	0.02
	Right forelimb lower	21.61	95.36	-188.58	-64.72	21.61	0.02
	Left forelimb foot	41.05	-97.94	-149.73	-94.57	41.05	0.04
	Right forelimb foot	41.05	97.94	-149.73	-94.57	41.05	0.04
	Left hindlimb lower	48.76	-114.55	-463.52	-53.22	48.76	0.05
	Left hindlimb lower	48.76	-114.55	-463.52	-53.22	48.76	0.05
	Left hindlimb upper	49.75	-73.26	-469.20	-26.54	49.75	0.05
	Left hindlimb upper1	49.75	-73.26	-469.20	-26.54	49.75	0.05
	Right hindlimb lower	48.76	114.55	-463.52	-53.22	48.76	0.05
	Right hindlimb upper	49.75	73.26	-469.20	-26.54	49.75	0.05
	Left hindlimb foot	64.78	-129.09	-426.49	-89.87	64.78	0.06
	Right hindlimb foot	64.78	129.09	-426.49	-89.87	64.78	0.06
Orobates Pabsti Limb Splayed Pose	Skull	254.40	-2.20	-72.34	-2.51	254.40	0.25
	Tail	202.79	-1.25	-613.22	4.85	202.79	0.20
	Torso	2401.06	-1.35	-315.88	-13.83	2401.06	2.40
	Right forelimb upper	38.30	65.28	-200.88	-40.76	38.30	0.04

	Right forelimb lower	21.91	114.27	-198.07	-38.69	21.91	0.02
	Right forelimb foot	36.54	176.77	-190.05	-44.66	36.54	0.04
	Left forelimb upper	53.95	-61.36	-199.76	-42.97	53.95	0.05
	Left forelimb lower	22.44	-117.79	-198.26	-38.45	22.44	0.02
	Left forelimb foot	41.05	-178.28	-190.93	-43.92	41.05	0.04
	Right hindlimb upper	48.95	70.00	-469.33	-26.58	48.95	0.05
	Right hindlimb lower	64.83	133.04	-468.67	-26.30	64.83	0.06
	Right hindlimb foot	64.78	191.25	-476.62	-32.08	64.78	0.06
	Left hindlimb upper	48.92	-72.64	-469.32	-26.57	48.92	0.05
	Left hindlimb lower	71.08	-133.20	-469.01	-26.17	71.08	0.07
	Left hindlimb foot	64.78	-193.89	-476.62	-32.08	64.78	0.06
Diadectes Tenuitectes Reference Pose	Tail	15358.44	-5.47	-1591.88	-137.13	15358.44	15.36
	Left femur	1212.97	-139.80	-1105.01	-117.80	1212.97	1.21
	Left fore foot	594.77	-239.78	-364.08	-322.50	594.77	0.59
	Left hind foot	885.78	-295.33	-1070.04	-310.22	885.78	0.89
	Left lower hindlimb	1825.88	-222.00	-1110.05	-197.57	1825.88	1.83
	Left upper forelimb	2031.84	-195.78	-470.70	-133.09	2031.84	2.03
	Left-lower-forelimb	2311.27	-163.44	-466.90	-237.53	2311.27	2.31
	Right femur	1327.04	149.05	-1100.17	-123.52	1327.04	1.33
	Right fore foot	565.69	218.48	-353.56	-321.98	565.69	0.57
	Right hind foot	828.43	293.61	-1058.48	-309.39	828.43	0.83
	Right lower hindlimb	1795.62	223.75	-1106.34	-201.37	1795.62	1.80
	Right upper forelimb	2414.73	181.47	-496.06	-130.05	2414.73	2.41
	Right lower forelimb	850.31	233.36	-467.91	-229.53	850.31	0.85
	Skull	6068.11	-12.23	-153.01	32.97	6068.11	6.07
	Torso	76698.44	-6.50	-747.86	-25.75	76698.44	76.70
Diadectes Tenuitectes Limb Splayed Pose	skull	5971.48	3.68	-151.19	11.98	5971.48	5.97
	Left femur	1458.79	-157.71	-1170.23	-119.83	1458.79	1.46
	Left front foot	548.33	-455.98	-437.43	-221.21	548.33	0.55

	Left hind foot	742.19	-467.89	-1133.94	-128.71	742.19	0.74
	Left lower forelimb	814.54	-329.79	-472.10	-182.09	814.54	0.81
	Left lower hindlimb	1814.99	-311.46	-1183.31	-129.59	1814.99	1.81
	Left upper forelimb	2876.06	-194.91	-455.79	-155.75	2876.06	2.88
	Right femur	1389.77	171.73	-1174.49	-120.94	1389.77	1.39
	Right front foot	505.97	467.24	-439.20	-223.05	505.97	0.51
	Right hind foot	785.44	473.71	-1137.20	-127.75	785.44	0.79
	Right lower forelimb	776.57	338.07	-466.35	-183.27	776.57	0.78
	Right lower hindlimb	1762.67	319.97	-1184.82	-128.69	1762.67	1.76
	Right upper forelimb	2852.16	203.35	-457.63	-157.79	2852.16	2.85
	Tail	14003.06	3.80	-1547.22	-152.78	14003.06	14.00
	Torso	83669.53	1.25	-729.95	-64.16	83669.53	83.67
Ophiacodon Uniformis Reference Pose	Skull	2252.95	-3.86	-198.79	20.72	2252.95	2.25
	Right hindlimb upper	89.60	69.39	-817.81	-96.91	89.60	0.09
	Right hindlimb lower	185.95	116.35	-874.47	-125.88	185.95	0.19
	Right hindlimb foot	215.82	142.02	-888.69	-185.38	215.82	0.22
	Left hindlimb upper	76.68	-95.79	-816.99	-96.16	76.68	0.08
	Left hindlimb lower	191.46	-145.89	-871.74	-122.91	191.46	0.19
	Left forelimb foot	222.98	-174.52	-886.39	-181.49	222.98	0.22
	Tail	1978.45	-16.11	-1085.89	-123.58	1978.45	1.98
	Torso	12776.11	-8.87	-555.15	-66.65	12776.11	12.78
	Right forelimb upper	61.21	87.81	-360.83	-91.71	61.21	0.06
	Right forelimb lower	97.15	137.36	-356.18	-122.15	97.15	0.10
	Right forelimb foot	143.02	121.73	-302.58	-176.87	143.02	0.14
	Left forelimb upper	59.14	-104.43	-359.43	-88.59	59.14	0.06
	Left forelimb lower	89.90	-152.45	-354.97	-117.11	89.90	0.09
	Left forelimb foot	134.83	-138.76	-300.11	-174.31	134.83	0.13
Ophiacodon Uniformis Limb Splayed Pose	Torso	13616.06	-6.21	-538.25	-65.41	13616.06	13.62
	Left hindlimb upper	138.94	-93.26	-822.09	-106.20	138.94	0.14

	Left fore foot	93.51	-277.42	-341.08	-71.29	93.51	0.09
	Left forelimb lower	120.17	-201.01	-348.86	-75.44	120.17	0.12
	Left hind foot	236.62	-315.96	-818.79	-97.32	236.62	0.24
	Left hindlimb lower	145.64	-205.92	-827.51	-106.85	145.64	0.15
	Left forelimb upper	70.31	-113.48	-354.02	-82.60	70.31	0.07
	Right femur	84.54	82.29	-827.77	-114.73	84.54	0.08
	Right fore foot	104.15	267.58	-350.12	-72.90	104.15	0.10
	Right forelimb lower	108.80	187.90	-358.21	-76.57	108.80	0.11
	Right hind foot	228.88	297.61	-830.34	-98.93	228.88	0.23
	Right hindlimb lower	150.65	186.22	-835.16	-107.92	150.65	0.15
	Right forelimb upper	64.61	104.15	-360.31	-83.59	64.61	0.06
	Skull	1677.98	-1.80	-172.44	28.17	1677.98	1.68
	Tail	2612.42	-7.45	-1076.70	-126.32	2612.42	2.61
Edaphosaurus Boanerges Reference Pose	Sail	18046.57	-6.32	-647.65	280.71	18046.57	18.05
	Skull	1162.99	0.69	-106.90	-15.15	1162.99	1.16
	Right hindlimb upper	233.15	116.30	-1043.93	-159.54	233.15	0.23
	Right hindlimb lower	174.20	177.93	-1067.79	-197.76	174.20	0.17
	Right hindlimb foot	205.51	210.34	-1016.59	-255.18	205.51	0.21
	Left hindlimb upper	254.82	-139.72	-1046.88	-155.09	254.82	0.25
	Left hindlimb lower	166.04	-210.36	-1067.49	-191.19	166.04	0.17
	Left hindlimb foot	275.95	-238.02	-1012.62	-243.51	275.95	0.28
	Tail	11022.57	-21.96	-1531.00	-171.88	11022.57	11.02
	Torso	54047.24	-5.98	-596.48	-81.31	54047.24	54.05
	Right forelimb upper	444.78	171.35	-308.48	-149.70	444.78	0.44
	Right forelimb lower	183.69	228.74	-300.80	-189.89	183.69	0.18
	Right forelimb foot	202.34	226.88	-214.89	-250.66	202.34	0.20
	Left forelimb upper	340.70	-171.62	-306.47	-138.96	340.70	0.34
	Left forelimb lower	289.74	-229.77	-301.14	-186.29	289.74	0.29
	Left forelimb foot	183.52	-226.26	-208.58	-246.55	183.52	0.18
Edaphosaurus Boanerges	Sail	31672.58	-7.49	-682.61	299.95	31672.58	31.67

Limb Splayed Pose	Skull	1008.01	-0.90	-99.09	0.75	1008.01	1.01
	Left forelimb foot	250.68	-417.92	-284.30	-125.56	250.68	0.25
	Left forelimb lower	216.11	-308.85	-288.43	-128.16	216.11	0.22
	Left forelimb upper	349.55	-185.62	-297.91	-133.70	349.55	0.35
	Left hindlimb foot	254.38	-305.06	-990.97	-175.66	254.38	0.25
	Left hindlimb lower	169.62	-230.11	-1046.92	-172.67	169.62	0.17
	Left hindlimb upper	384.02	-113.07	-1050.91	-152.57	384.02	0.38
	Right forelimb foot	251.45	420.79	-284.59	-106.18	251.45	0.25
	Right forelimb lower	214.31	312.10	-287.12	-112.68	214.31	0.21
	Right forelimb upper	428.88	180.29	-298.19	-125.61	428.88	0.43
	Right hindlimb foot	276.22	308.52	-992.05	-161.97	276.22	0.28
	Right hindlimb lower	154.69	234.26	-1047.68	-161.41	154.69	0.15
	Right hindlimb upper	395.74	116.08	-1049.99	-147.71	395.74	0.40
	Tail	11761.79	-3.45	-1565.53	-169.14	11761.79	11.76
	Torso	56095.56	-0.08	-606.51	-68.77	56095.56	56.10
Dimetrodon Milleri Reference Pose	Dimetrodon1. Skull	2407.51	-0.72	-150.14	-14.45	2407.51	2.41
	Dimetrodon10. Right hindlimb upper	291.84	111.52	-881.34	-101.59	291.84	0.29
	Dimetrodon11. Right hindlimb lower	168.43	152.13	-954.41	-129.52	168.43	0.17
	Dimetrodon12. Right hindlimb foot	288.67	185.70	-986.16	-179.96	288.67	0.29
	Dimetrodon13. Left hindlimb upper	217.64	-100.02	-877.31	-99.89	217.64	0.22
	Dimetrodon14. Left hindlimb lower	278.90	-146.74	-966.19	-129.68	278.90	0.28
	Dimetrodon15. Left hindlimb foot	260.73	-180.74	-991.67	-180.00	260.73	0.26
	Dimetrodon16. Sail	6815.34	4.17	-560.98	132.06	6815.34	6.82
	Dimetrodon2. Tail	1784.54	0.89	-1232.05	-122.04	1784.54	1.78
	Dimetrodon3. Torso	23045.42	2.92	-528.30	-75.59	23045.42	23.05
	Dimetrodon4. Right forelimb upper	194.41	152.45	-331.13	-90.31	194.41	0.19

	Dimetrodon5. Right forelimb lower	221.67	209.32	-308.31	-133.20	221.67	0.22
	Dimetrodon6. Right forelimb foot	110.45	213.68	-223.76	-195.69	110.45	0.11
	Dimetrodon7. Left forelimb upper	165.68	-145.68	-335.67	-90.32	165.68	0.17
	Dimetrodon8. Left forelimb lower	209.24	-204.79	-313.12	-133.95	209.24	0.21
	Dimetrodon9. Left forelimb foot	119.92	-208.82	-231.52	-196.37	119.92	0.12
Dimetrodon Milleri	Skull	2218.92	0.38	-152.01	-9.04	2218.92	2.22
Limb Splayed Pose	Left forelimb foot	133.66	357.73	-303.79	-77.58	133.66	0.13
	Left forelimb lower	137.50	260.69	-315.11	-80.78	137.50	0.14
	Left forelimb upper	288.32	133.19	-324.88	-88.34	288.32	0.29
	Left hindlimb foot	148.65	343.26	-855.32	-97.98	148.65	0.15
	Left hindlimb lower	249.08	245.79	-891.44	-94.56	249.08	0.25
	Left hindlimb upper	249.71	107.01	-881.98	-93.25	249.71	0.25
	Right forelimb foot	138.31	-355.87	-296.62	-83.55	138.31	0.14
	Right forelimb lower	135.10	-258.56	-310.01	-85.09	135.10	0.14
	Right forelimb upper	259.04	-134.21	-322.12	-93.33	259.04	0.26
	Right hindlimb foot	139.00	-349.38	-846.83	-104.25	139.00	0.14
	Right hindlimb lower	251.78	-253.12	-885.45	-99.22	251.78	0.25
	Right hindlimb upper	235.05	-112.67	-876.35	-96.24	235.05	0.24
	Sail	6551.28	-2.83	-590.71	135.68	6551.28	6.55
	Tail	2091.40	-3.54	-1262.58	-121.49	2091.4	2.09
	Torso	21947.21	-0.88	-539.50	-75.93	21947.21	21.95

Dinodontosaurus Turpior	Skull	15527.62	-2.68	-213.71	39.61	15527.62	15.53
Reference Pose	Right hindlimb lower	2503.10	187.97	-1345.75	-310.65	2503.10	2.50
	Right hindlimb foot	2041.24	205.37	-1353.54	-464.06	2041.24	2.04
	Left hindlimb upper	3384.04	-241.71	-1343.29	-122.49	3384.04	3.38
	Right hindlimb upper	3384.04	181.98	-1343.29	-122.49	3384.04	3.38
	Left hindlimb lower	2537.13	-248.50	-1342.54	-309.13	2537.13	2.54

	Left hindlimb foot	2026.89	-262.15	-1351.40	-462.26	2026.89	2.03
	Tail	1262.33	-36.44	-1673.92	-90.03	1262.33	1.26
	Torso	166209.71	-21.96	-950.36	37.51	166209.71	166.21
	Left forelimb upper	4444.52	-252.26	-651.09	-171.62	4444.52	4.44
	Right forelimb upper	4444.52	252.26	-651.09	-171.62	4444.52	4.44
	Left forelimb lower	2850.15	-310.13	-700.17	-306.92	2850.15	2.85
	Right forelimb lower	2850.15	310.13	-700.17	-306.92	2850.15	2.85
	Left forelimb foot	2528.32	-249.65	-579.34	-467.33	2528.32	2.53
	Right forelimb foot	2528.32	249.65	-579.34	-467.33	2528.32	2.53
Dinodontosaurus Turpior Limb Splayed Pose	Right forelimb foot	2319.13	665.60	-501.46	-181.99	2319.13	2.32
	Skull	16411.50	-1.55	-209.52	38.78	16411.50	16.41
	Left forelimb foot	2478.79	-681.15	-474.31	-182.32	2478.79	2.48
	Left forelimb lower	3090.34	-481.38	-571.54	-172.92	3090.34	3.09
	Left forelimb upper	6310.56	-289.16	-565.99	-163.11	6310.56	6.31
	Left hindlimb foot	1885.31	-662.78	-1235.91	-33.58	1885.31	1.89
	Left hindlimb lower	3035.98	-443.26	-1277.22	-36.68	3035.98	3.04
	Left hindlimb upper	3776.07	-221.66	-1332.53	-5.57	3776.07	3.78
	Right forelimb lower	2744.13	466.65	-590.73	-175.09	2744.13	2.74
	Right forelimb upper	5912.76	262.72	-575.02	-161.16	5912.76	5.91
	Right hindlimb foot	1467.93	629.44	-1253.27	-34.68	1467.93	1.47
	Right hindlimb lower	3724.19	419.29	-1293.12	-36.05	3724.19	3.72
	Right hindlimb upper	3810.60	188.98	-1333.55	-0.93	3810.60	3.81
	Tail	1746.83	-32.03	-1655.73	-74.04	1746.83	1.75
	Torso	164991.31	-16.68	-943.62	38.95	164991.3	165.0
Scaloposaurus punctatus Reference Pose	Left forelimb foot	1.15	-46.82	-87.72	-57.61	1.15	0.00
	Left forelimb lower	0.91	-45.65	-101.05	-40.05	0.91	0.00
	Left forelimb upper	1.70	-29.20	-91.57	-24.26	1.70	0.00
	Left hindlimb foot	1.15	-46.89	-150.80	-59.20	1.15	0.00
	Left hindlimb upper	1.53	-29.28	-164.33	-15.62	1.53	0.00
	Lower hindlimb left	1.26	-42.64	-157.94	-37.76	1.26	0.00
	Trunk	90.65	-4.61	-118.89	-16.29	90.65	0.09
	Right forelimb foot	1.15	37.53	-88.38	-58.00	1.15	0.00

	Right forelimb lower	0.91	36.44	-100.90	-40.18	0.91	0.00
	Right forelimb upper	1.70	19.51	-91.60	-24.22	1.70	0.00
	Right hindlimb foot	1.15	37.47	-150.65	-59.58	1.15	0.00
	Right hindlimb lower	1.26	32.97	-158.40	-35.29	1.26	0.00
	Right hindlimb upper	1.53	19.02	-165.12	-14.55	1.53	0.00
	Scaloposaurus Skull	19.98	-2.22	-31.80	2.50	19.98	0.02
	Scaloposaurus Tail	0.20	-5.38	-186.92	-28.25	0.20	0.00
			0.00	0.00	0.00	0.00	0.00
Scaloposaurus punctatus	Left forelimb foot	1.15	-90.19	-81.12	-17.01	1.15	0.00
Limb Splayed Pose	Left forelimb lower	0.91	-63.33	-82.78	-17.14	0.91	0.00
	Left forelimb upper	1.70	-31.87	-82.31	-23.70	1.70	0.00
	Left hindlimb foot	1.15	-98.73	-172.00	-23.20	1.15	0.00
	Left hindlimb upper	1.53	-35.52	-172.94	-15.62	1.53	0.00
	Lower hindlimb left	1.26	-70.14	-172.29	-23.40	1.26	0.00
	Trunk	90.65	-4.61	-118.89	-16.29	90.65	0.09
	Right forelimb foot	1.15	82.25	-83.58	-16.04	1.15	0.00
	Right forelimb lower	0.91	55.46	-84.02	-15.87	0.91	0.00
	Right forelimb upper	1.70	24.10	-83.09	-23.67	1.70	0.00
	Right hindlimb foot	1.15	90.40	-172.92	-26.02	1.15	0.00
	Right hindlimb lower	1.26	60.67	-173.24	-25.38	1.26	0.00
	Right hindlimb upper	1.53	26.52	-172.90	-14.55	1.53	0.00
	Scaloposaurus Skull	19.98	-2.22	-31.80	2.50	19.98	0.02
	Scaloposaurus Tail	0.20	-5.38	-186.92	-28.25	0.20	0.00
Procynosuchus delaharpeae	L forelimb foot	17.85	-75.88	-161.02	-168.19	17.85	0.02
Reference Pose	L forelimb lower	14.30	-79.21	-188.00	-137.03	14.30	0.01
	L forelimb upper	13.84	-57.60	-197.45	-97.45	13.84	0.01
	L hindlimb foot	13.60	-75.24	-427.91	-167.54	13.60	0.01
	L hindlimb lower	7.43	-76.33	-456.53	-135.40	7.43	0.01
	L hindlimb upper	19.10	-46.12	-470.52	-103.11	19.10	0.02
	R forelimb foot	17.85	107.70	-146.32	-157.13	17.85	0.02
	R forelimb lower	14.30	109.85	-173.49	-126.03	14.30	0.01
	R forelimb upper	13.84	84.20	-186.40	-90.00	13.84	0.01
	R hindlimb foot	13.60	109.37	-425.63	-168.63	13.60	0.01
	R hindlimb lower	7.43	106.82	-453.50	-135.92	7.43	0.01

	R hindlimb upper	19.10	73.71	-465.43	-105.71	19.10	0.02
	Skullduplicate+	153.19	10.10	-68.60	-25.22	153.19	0.15
	Tail	67.88	18.01	-607.71	-95.34	67.88	0.07
	Trunk	2468.05	13.74	-325.69	-74.18	2468.05	2.47
Procynosuchus delaharpeae Limb Splayed Pose	L forelimb foot	17.85	-181.14	-191.94	-104.14	17.85	0.02
	L forelimb lower	14.30	-130.13	-198.14	-102.68	14.30	0.01
	L forelimb upper	13.84	-64.13	-197.45	-97.45	13.84	0.01
	L hindlimb foot	13.60	-157.60	-471.92	-118.57	13.60	0.01
	L hindlimb lower	7.43	-111.17	-469.05	-112.45	7.43	0.01
	L hindlimb upper	19.10	-52.65	-470.52	-103.11	19.10	0.02
	R forelimb foot	17.85	203.02	-185.28	-96.91	17.85	0.02
	R forelimb lower	14.30	149.55	-189.17	-93.72	14.30	0.01
	R forelimb upper	0.23	78.55	-186.85	-90.11	0.23	0.00
	R hindlimb foot	13.60	179.47	-461.41	-120.09	13.60	0.01
	R hindlimb lower	7.43	129.67	-460.14	-112.87	7.43	0.01
	R hindlimb upperduplicate	19.10	67.19	-465.43	-105.71	19.10	0.02
	R upper forelimb	13.84	82.43	-191.59	-89.57	13.84	0.01
	Skullduplicate+	153.19	1.94	-68.60	-25.22	153.19	0.15
	Tail	67.88	11.48	-607.71	-95.34	67.88	0.07
	Trunk	2466.49	7.21	-325.69	-74.17	2466.49	2.47

Figure 1. A digitized skeletal model of the stem amniote *Diadectes tenuitectes* and a convex hull model of its major body segments.

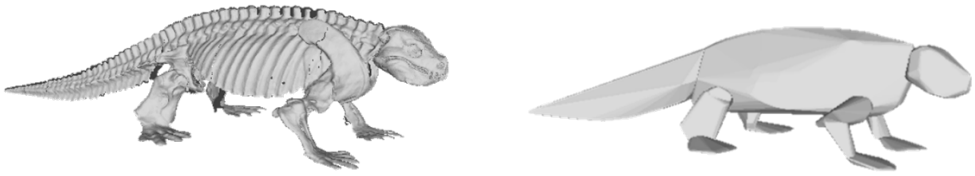

Figure 2. Partial phylogenetic tree of Tetrapoda showing relationships between selected taxa.

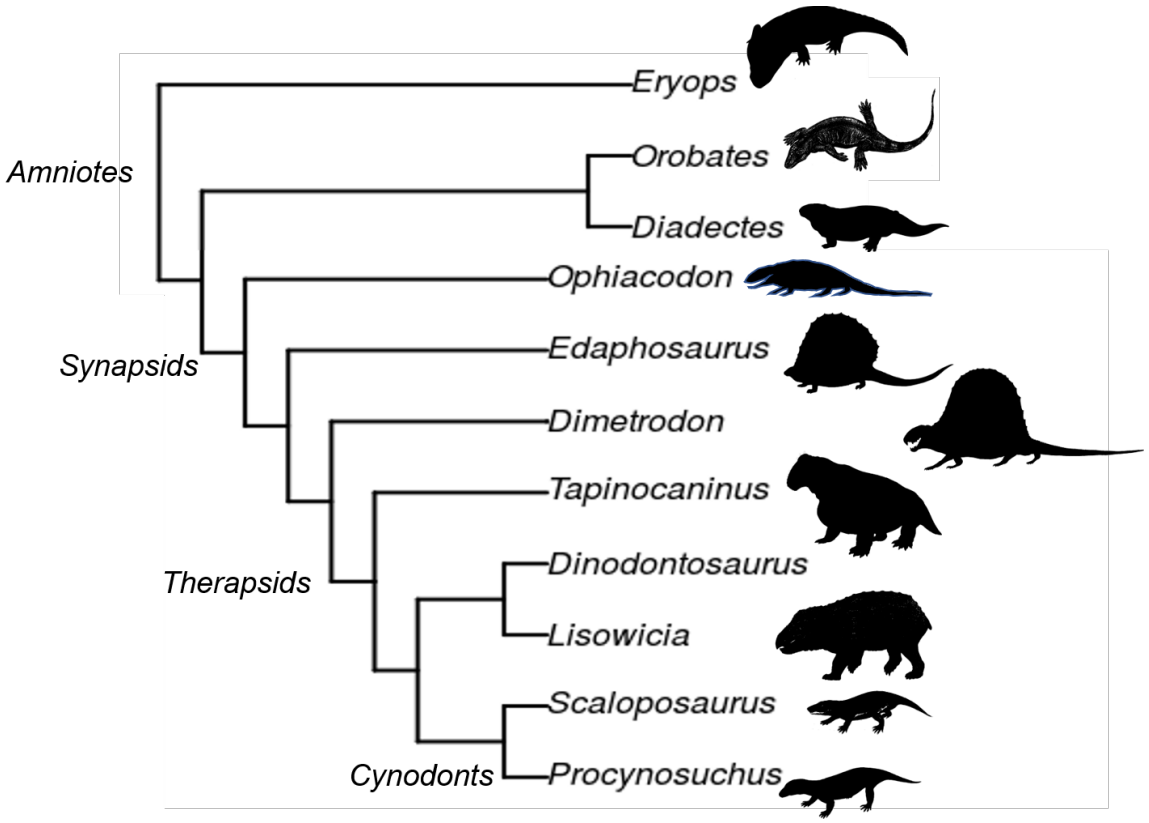

Figure 3. Skeletal reconstructions and minimum convex hull representations of the nine specimens used for volumetric modeling.

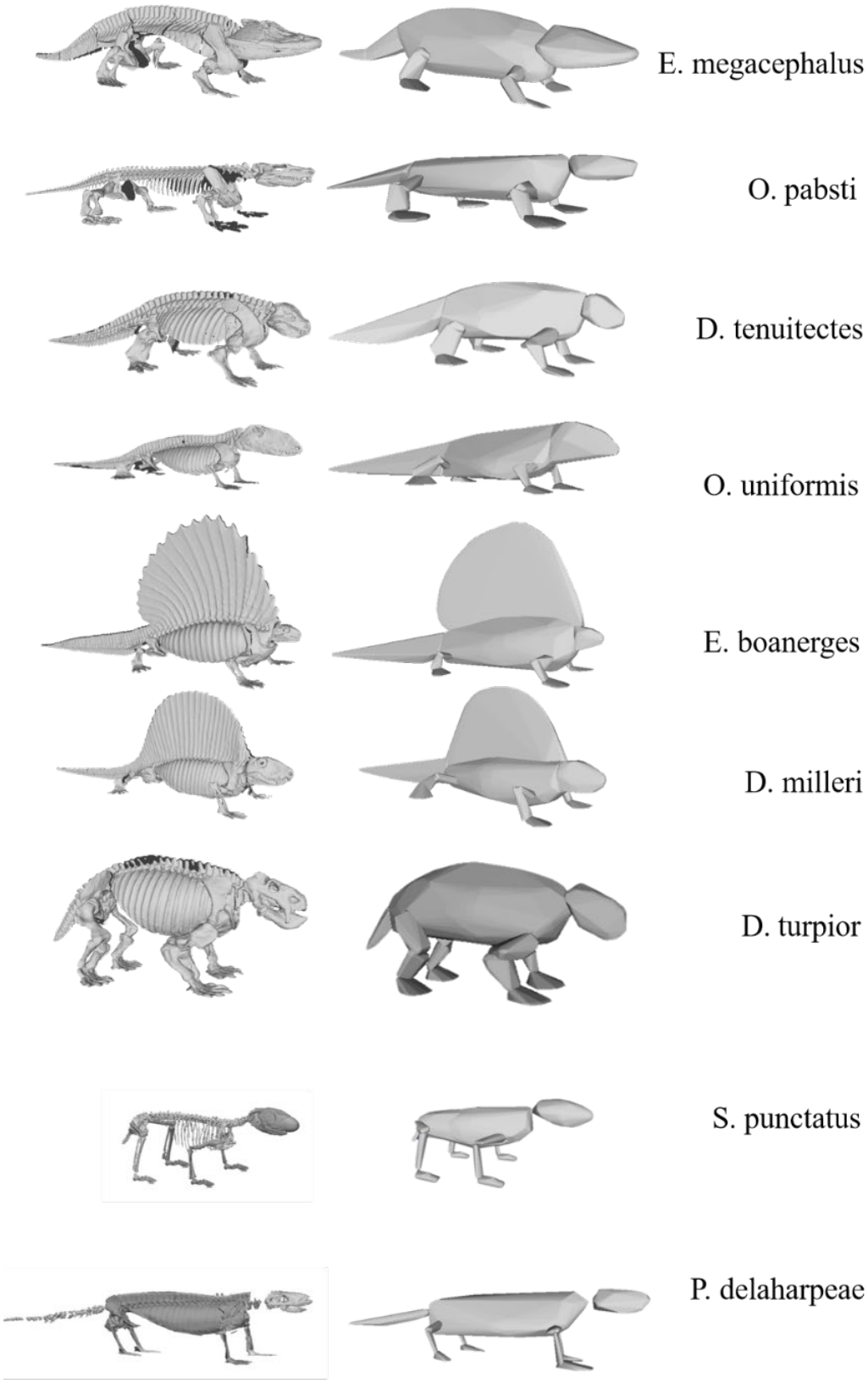

Figure 4. a, Three-dimensional photogram model of femur, *D. turpior*. b, Two-dimensional projection obtained from using 3-Matic sketch function, permitting measurement of bone length.

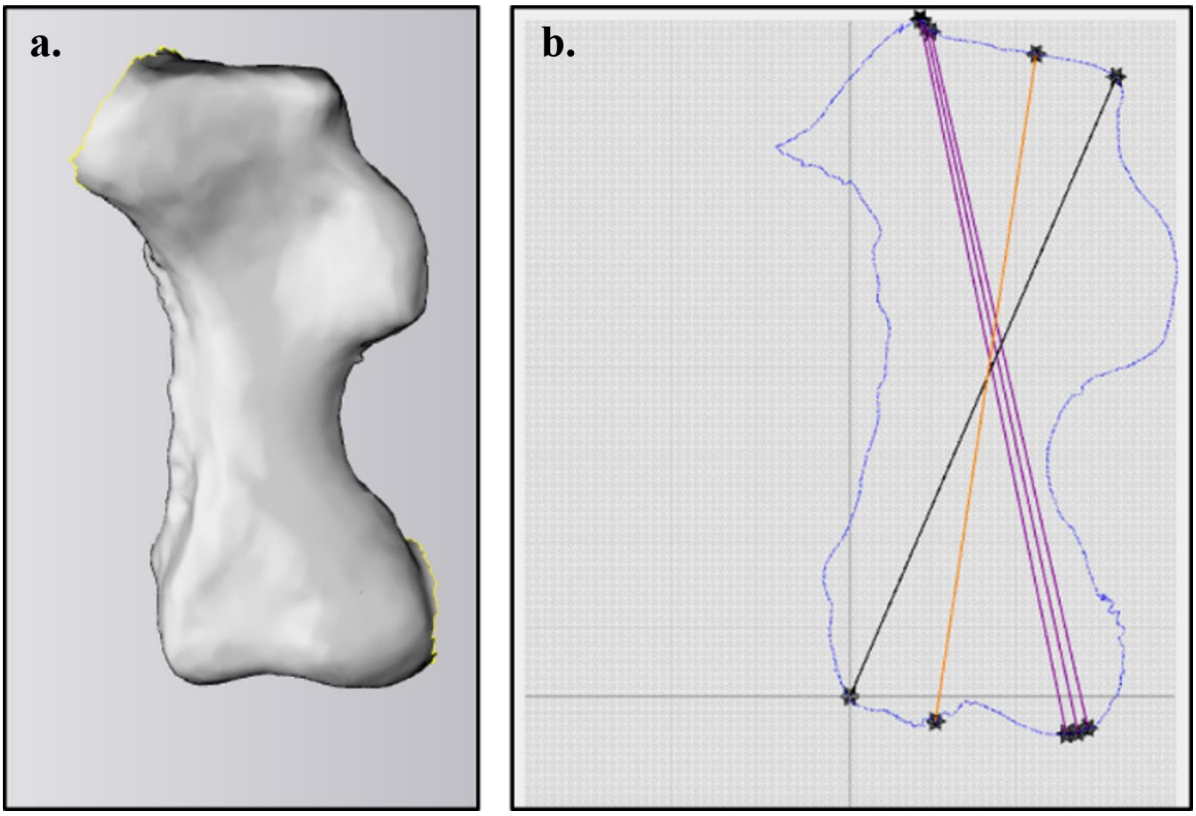

Figure 5. Geometric representation of center of mass, glenoid, and acetabulum with line segments used for calculation.

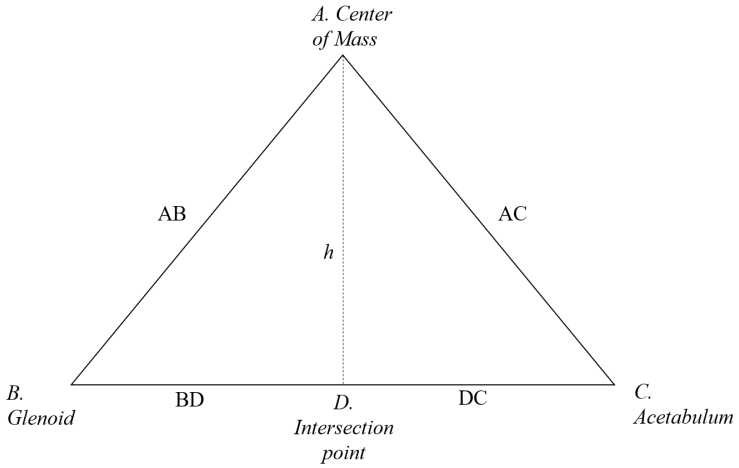

Figure 6. Center of mass is referenced (1) as a fraction of the distance cranial to the glenoid fossa from the acetabulum and (2) as distance cranial to the acetabulum normalized by femur length.

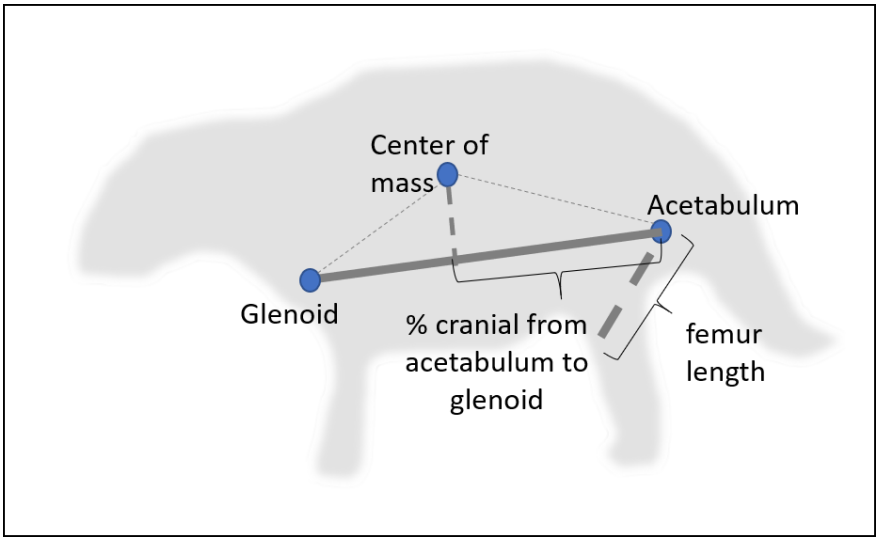

Figure 7. Body mass estimate results: blue bars represent limb-scaling equations based on combined humerus and femur circumference, individual humerus, individual femur, reptilian only model, and mammalian only model after Campione and Evans (2012), and quadratic form after Campione (2017); yellow bars represent volumetric density estimates based on the minimum convex hull multiplied by a minimum density value of 893 kg/m3, a maximal density value of 1080 kg/m3, and a neutral density of 1000 kg/m3 plus a 21% expansion after Sellers et al (2012).

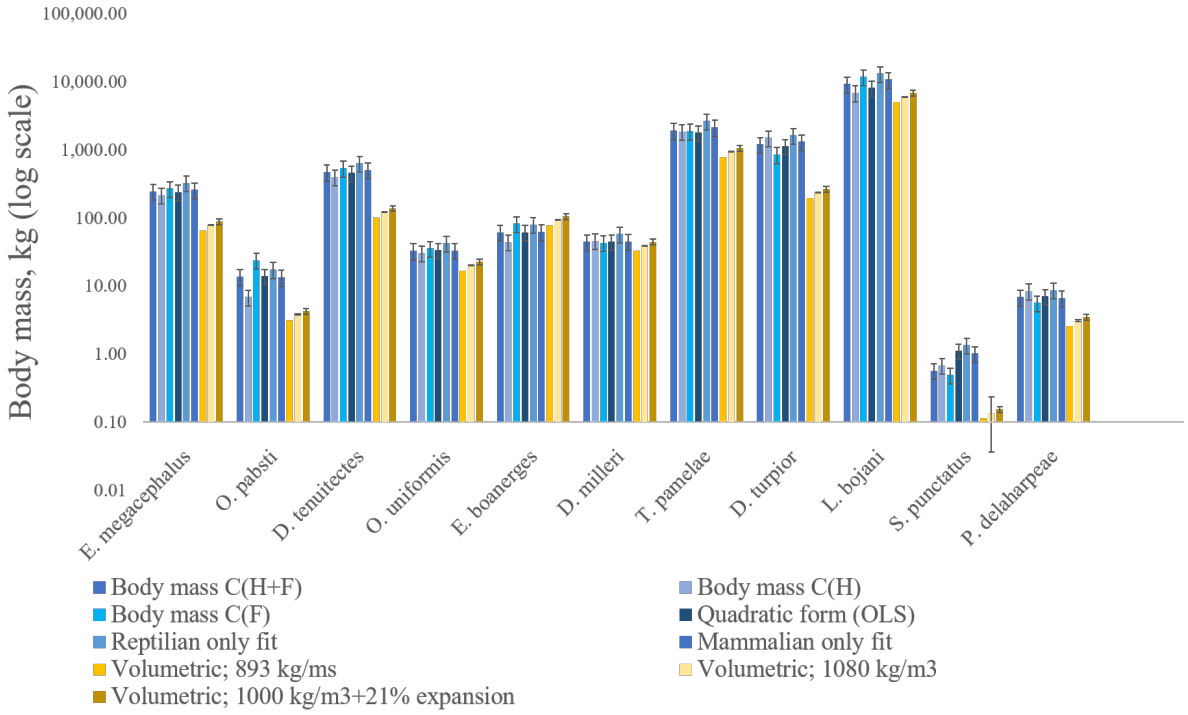

Figure 8. Center of mass position measured cranially from the acetabulum to the glenoid; bounds indicate 40 and 60%. The only outlier to this constraint is *Scaloposaurus* (7#%?), a likely juvenile.

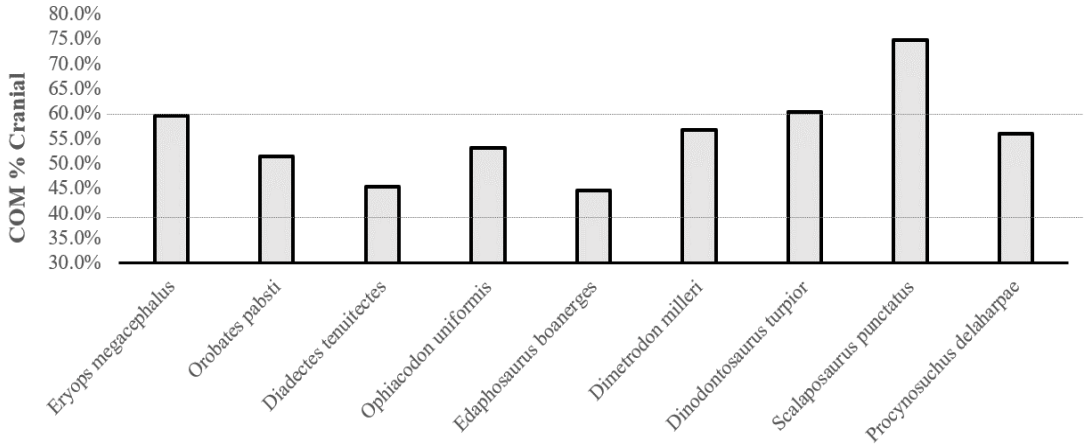

Figure 9. a., Linear relationship between skull to tail mass ratio and center of mass position ($p = 0.00016$, $r^2 = 0.868$) b., Relationship after correcting for phylogeny using the phylogenetic independent contrasts method position ($p = 0.00005$, $r^2 = 0.904$) (Revell, 2012). A strong positive trend is observed associating high skull to tail mass ration with more anterior center of mass position.

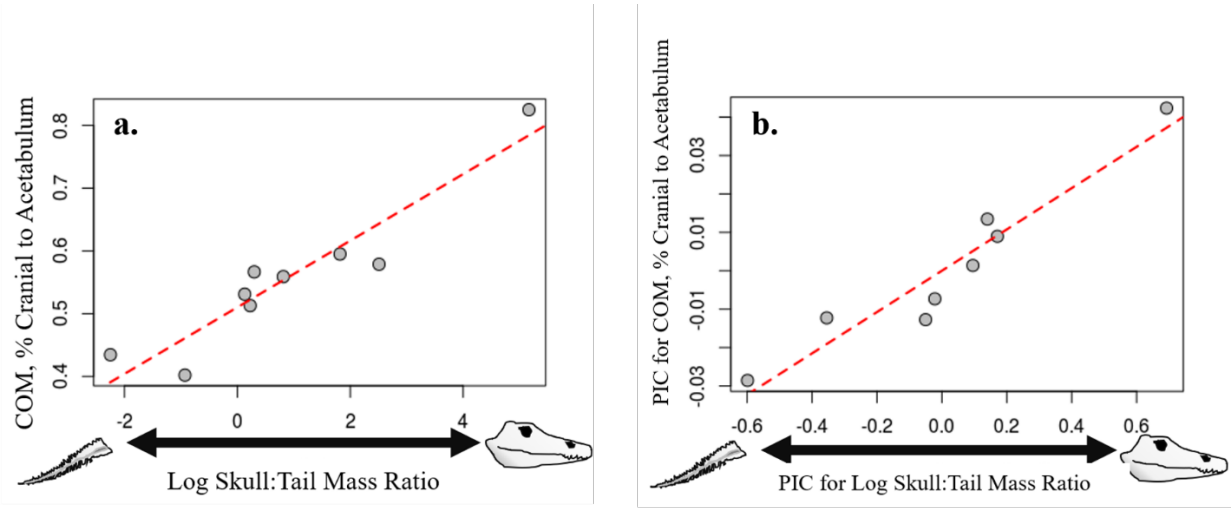

Figure 10. Center of mass results normalized by femur length. Dashed line indicates unity, hypothesized as upper limit to permit static stability during bipedal locomotion. Values observed here range from approximately 1.5-2.1.

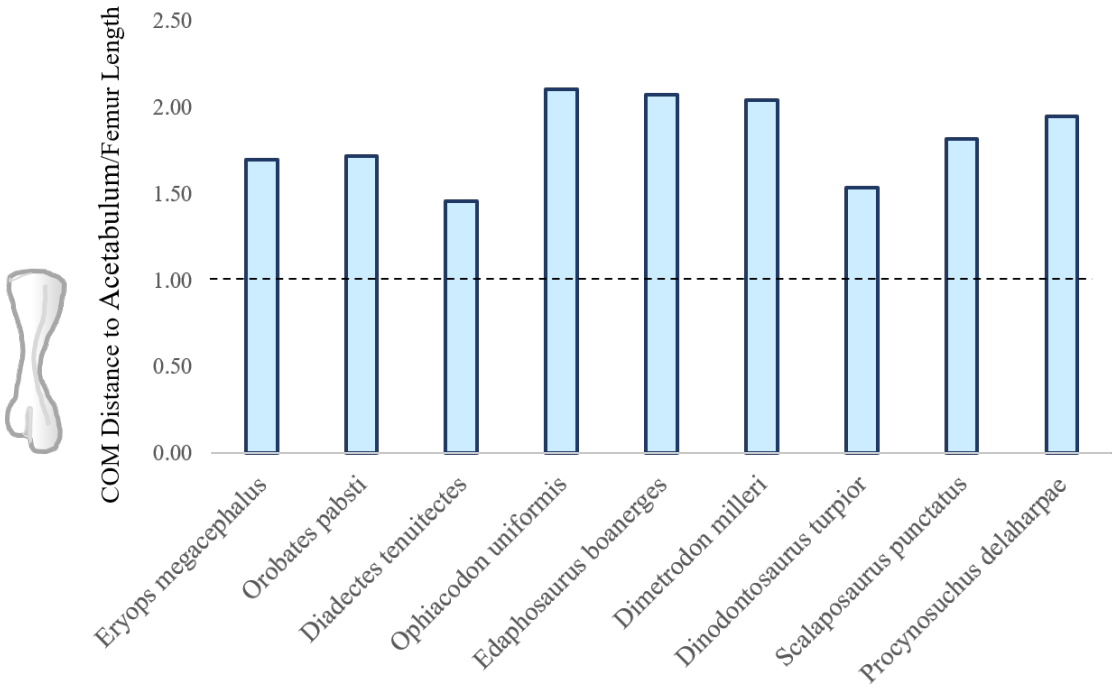

Figure 11. Skeletal reconstructions showing overlay of a., Minimum convex hull (Volume=0.219 m^3, Mass @ 1000 kg/m^3=219.1 kg); b., Min. convex hull scaled up by 21% (Volume=0.265 m^3, Mass @ 1000 kg/m^3=265.35 kg); c., Min. convex hull scaled up by 352% as proposed by the limb scaling estimation method (Volume=0.984 m^3,Mass @ 1000 kg/m^3=984 kg).

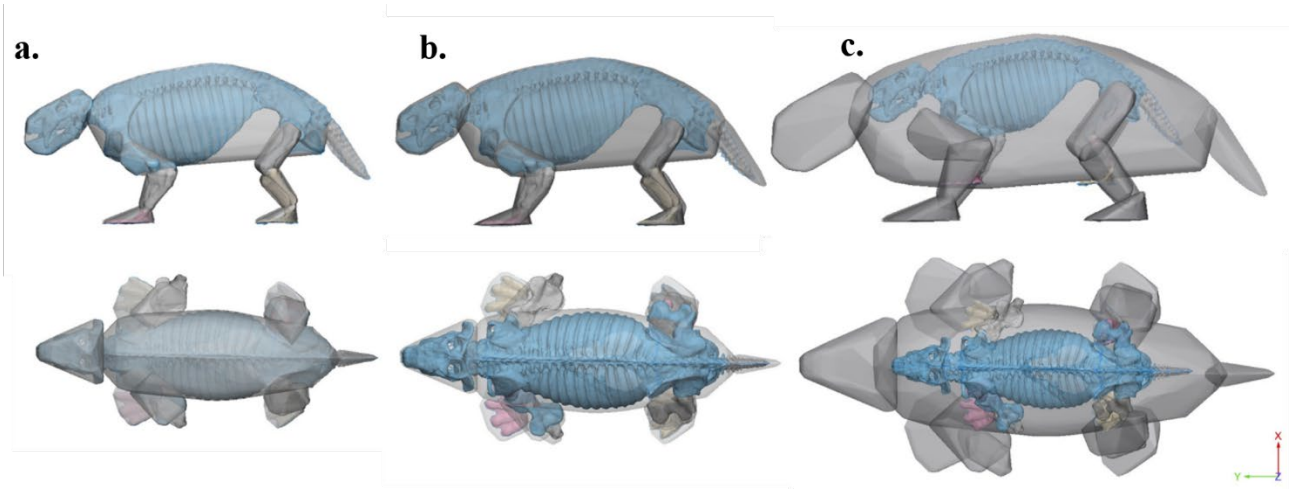

Figure 12. Comparison of stylopodial robustness among fossil dataset with extant mammal and reptile specimens used to generate limb scaling curves in Campione & Evans (2012). Outlier data points from the extant tetrapod sets display functional specialization; the highest values of humerus robustness (*P. breweri* and *C. cristata*) are from specimens adapted for fossorial habit, while the highest values of femur robustness (*P. groenlandica* and *A. pusillus*) are from specimens adapted for aquatic locomotion.